9950 - 636

AS&E

American Science and Engineering, Inc.
955 Massachusetts Avenue
Cambridge, Massachusetts 02139
617-868-1600 Telex 921-458

30 OCTOBER 1981

ASE-4672

STARPROBE: A DESIGN STUDY FOR AN X-RAY IMAGING INSTRUMENT

UNDER CONTRACT NUMBER 955928
AS PART OF NASA CONTRACT NAS7-100

PREPARED FOR:
JET PROPULSION LABORATORY
CALIFORNIA INSTITUTE OF TECHNOLOGY
4800 Oak Grove Drive
Pasadena, California 91103

ASE-4672

STARPROBE: A Design Study for an X-Ray Imaging Instrument

Prepared for:

Jet Propulsion Laboratory
California Institute of Technology
4800 Oak Grove Drive
Pasadena, California 91103

Under Contract Number 955928
as part of NASA Contract NAS7-100

Prepared by:

American Science and Engineering, Inc.
Space Systems Division
37 Broadway
Arlington, Massachusetts 02174

October 30, 1981

Prepared and Approved by:

John M. Davis

John M. Davis
Program Manager

FOREWORD

This document is the Final Report of a design study of X-ray imaging techniques applicable to the STARPROBE mission. The study was performed by American Science and Engineering (AS&E) Space Systems Division, under contract to the Jet Propulsion Laboratory (JPL). Technical direction at JPL was given by Dr. J.H. Underwood and Mr. J.E. Randolph.

At AS&E the study participants were Dr. J.M. Davis, Dr. R.C. Chase, Dr. N.G. Leter, Mr. J. Ortendahl and Mr. R. Mastronardi.

TABLE OF CONTENTS

1.0 INTRODUCTION

STARPROBE is a NASA proposed multi-disciplinary mission to study the sun from the perspective of a close encounter. The current trajectory has perihelion occurring at 4 $R_\odot$ or 3 $R_\odot$ above the surface of the photosphere. This trajectory will permit measurement of the solar quadrupole moment (J_2), in situ measurements of the particle and field environment near the sun and imaging observations with a resolution unobtainable from earth orbit.

As a preliminary to the mission, studies were commissioned to establish whether imaging experiments, which must look at the sun, could be carried out from STARPROBE. As a result of proposals received from a competitive RFP, American Science and Engineering, Inc. (AS&E) and Ball Aerospace Systems Division (BASD) were selected to perform studies. By mutual agreement between JPL and the two contractors AS&E's effort was directed to the study of X-ray imaging (grazing incidence optics) while BASD would study visible and UV imaging[1] (normal incidence optics).

The scientific objectives established for the X-ray instrument have been established by the STARPROBE Ad Hoc Imaging Committee.[2] They are:

1. What is the thermal structure of coronal loops? How important is mass flow in loops, and how is mass exchange between the chromosphere and coronal loops accomplished? Can evidence for heating by current dissipation or reconnection be discerned from the thermal structure of loops?

2. What is the structure of coronal bright points? What role do they play in the transport of mass into the solar wind, and in the emergence of magnetic flux? What processes heat bright points and supply the energy for their flare-like behavior?

3. What is the transition region structure in coronal holes (open field regions)? What processes are responsible for mass transport? Are abundance gradients observable in the low corona in holes?

4. How does the energy budget of the corona differ in coronal holes, and in strong and weak field regions?

To provide observations that will meet these objectives the X-ray instrument must be capable of 1 arc second angular resolution. There is also a requirement for obtaining rapid exposures, since during the perihelion passage the sub-probe point will be moving at approximately 7 arc seconds per second. Since plasma diagnostics require images through at least two different filters these images must be acquired close together in time if uncertainties arising from spatial misalignments are not to be introduced into the analysis.

Therefore, during this study we have:

1. Developed a design for the X-ray optics which we belive satisfies the scientific requirements and can be accommodated within the STARPROBE baseline design;

2. Performed structural and thermal analyses which describe the environment that must be maintained within the instrument package to meet the tolerances of the instrument;

3. Studied the X-ray and thermal properties of the telescope prefilters which have to withstand the direct and indirect thermal loading at perihelion;

4. Estimated the exposure times required for the telescope design developed under Paragraph 1.

2.0 MIRROR DESIGN

2.1 General Requirements

The primary objective of the X-ray imaging telescope on STARPROBE is the acquisition of very high spatial resolution observations during the spacecraft's perihelion passage. Current grazing incidence telescopes have achieved 1 arc second resolution and the next generation may, under the most optimistic scenario, push this limit to 0.2 arc seconds.[3] However, the STARPROBE telescope will have to operate within a severe thermal environment and consequently it would be over-optimistic to require a telescope performance significantly better than 1 arc second.

To place this goal in perspective 1 arc second observations, carried out from earth orbit, correspond to a spatial resolution of 720 km on the sun's surface. The most optimistic resolution attainable from earth orbit this century, may be 0.2 arc seconds, which corresponds to 144 km on the sun. However the STARPROBE telescope with one arc second resolution carried to within three solar radii of the solar surface could resolve features with a 10 km separation, i.e., an order of magnitude improvement over the best that can be hoped for from earth orbit.

The system resolution depends on the performance of both the telescope and its detector. That is the size of the detector pixel must be smaller than the desired resolution, in the focal plane, if the detector itself is not to limit resolution. In practice the detector size is fixed and the focal length of the telescope is chosen to match the detector pixel with the resolution requirement. However for STARPROBE the total length of the instrument is also restricted and it is impossible to match detectors and focal lengths to obtain the desired one arc second resolution with a single mirror telescope. Therefore we have adopted a two mirror solution in which a second grazing incidence mirror is used to bend the focused beam from the primary image. This optical system has been referred to as a diverging relay optics

telescope[3] since the second reflection occurs before the primary focus and performs the same function as a diverging lens in a normal incidence optical system.

Because of the fixed detector size there exists a conflict between resolution and field of view, i.e., as the resolution increases the field of view decreases. This poses a possible problem for the interpretation of the highest resolution images in terms of the features which can be observed from earth. The double grazing incidence mirror system we have adopted aggravates this problem but also provides a solution. The problem is that ray tracing indicates that the resolution of the secondary image falls off rapidly with off-axis angle, more rapidly than for a single mirror system and this effect may limit the field of view before the detector limit is reached. Although experience gained comparing predicted blur circle radii with actual observations for single grazing incidence mirror systems suggests that this problem might be overstated.[4] However if a second detector is provided at the primary focus it can be used for locating the magnified images within the framework of the target area. Therefore our baseline design provides for imaging at both the primary and secondary foci.

2.2 Design Parameters

The STARPROBE X-ray telescope has been designed to meet the following criteria:

1. A sufficient collecting area to take rapid exposures,
2. An effective on-axis (within 1 arc min) resolution of 1 arc second, and
3. A field of view of sufficient size so that the images can be interpretable in terms of the features seen from earth orbit.

The second and third requirements are, in part, established by the size of the detector which we have taken as an 800 x 800 element CCD

with 15 micron cells. Therefore the images will have a square format with a side of 1.2 cm. This selection is somewhat arbitrary but reflects existing technology. Improvements in this area will result in similar improvements in the performance of the STARPROBE X-ray telescope.

In Table 2-1 we show the maximum field of view, allowed by this detector, as a function of the focal length of a single mirror system. For the range of focal lengths, which could be contained within the STARPROBE spacecraft, 0.5 and 1.75 m, the field of view ranges from 82.5 to 23.6 arc minutes. Typically X-ray mirrors are designed with field of view of order 1° and any of these values could form the basis for a useful X-ray mirror design.

TABLE 2-1 FIELDS OF VIEW

Focal Length Meters	Detector arc-minutes	Equivalent Field of View arc seconds	Detector Resolution at Perihelion - kms
0.50	82.5	69.3	62.6
0.75	55.0	46.2	41.7
1.00	41.2	34.6	31.3
1.25	33.0	27.7	25.0
1.50	27.5	23.1	20.8
1.75	23.6	19.8	17.9

Two instructive parameters included in the Table are the equivalent field of view which is the size of the perihelion field when viewed from the earth and the spatial resolution of a detector element at perihelion. Inspection of Table 2-1 shows that even the longest focal length, single mirror system, which could be contained within STARPROBE, does not provide sufficient resolution and that even so the equivalent field of view for this the longest focal length system is quite small.

Our proposed solution is to add a stage of magnification by introducing a second set of grazing incidence mirrors. Using the three shorter focal lengths of Table 2-1 and magnifications between 3 and 10, it is possible to fit effective focal lengths of 2.00 to 5.00 m within the instrument package (Table 2-2).

TABLE 2-2

Primary Focal Length Meters	Magnification	Effective Focal Length Meters	FIELDS OF VIEW Detector arc min	Perihelion Viewed from Earth arc seconds	Resolution (Detector Pixel) kms
0.5	4	2.0	20.6	17.3	15.6
	6	3.0	13.7	11.5	10.4
	8	4.0	10.3	8.7	7.8
0.75	4	3.0	13.7	11.5	10.4
	6	4.5	9.2	7.7	6.9
1.00	3	3.0	13.7	11.5	10.4
	5	5.0	8.2	6.9	6.3

Any of these combinations would provide adequate resolution in principle and although the secondary field is small, the primary image can be used for placing the secondary image in perspective.

From this group of telescopes we have undertaken two detailed designs for comparison purposes. We have selected an effective focal length of 3 m which provides a resolution element of 10 km and compared the performance of X4 and X6 magnifiers with 0.5 and 0.75 m primary focal lengths.

2.3 Design of the Secondary

In principle secondary grazing incidence mirrors can be designed to be placed either behind the primary focus as an analog of the eyepiece in

a simple astronomical telescope or in front of the primary focus where they act as a Barlow lens. The latter approach has three advantages, namely:

1. The primary focussed X-rays are bent through a smaller angle to reach the secondary focus, thus minimizing reflection losses and maximizing collecting area.

2. The closer the secondary mirror is located to the primary, the smaller is the displacement from the nominal ray of the off-axis rays. This results in an improved off-axis response.

3. A shorter overall length is possible for a given object distance and magnification.

The secondary grazing incidence mirrors of this approach have hyperboloid-hyperboloid surfaces and the stages in the design of the telescope are as follows:

1. The primary is chosen as a Wolter Type I with paraboloid-hyperboloid surfaces. Its dimensions are governed by the focal length and grazing angle which it is wished to use. Larger grazing angles give greater collecting areas but also limit the short wavelength performance. As a compromise we have chosen a grazing angle of 1.2 degrees which gives good performance with a nickel surfaced telescope down to 6 Å. The length of the elements of the mirror are made equal to the mirror diameter which increases collecting area at the expense of off-axis performance.

2. The object distance of the secondary mirror, that is the location of the secondary mirror in front of the primary focus, is established such that the overall length of the system is 1.75 m. This in turn fixes the radii of secondary mirror.

3. Element lengths of the secondary mirror are made just large enough to catch all the on-axis rays. Increasing the element length will increase the collecting area but only at the expense of degrading the off-axis performance.

The results of this analysis are shown in Table 2-3. There are two significant differences between the designs. First, although the collecting area is higher for the lower magnification, there is less fall-off in collecting area with off-axis angle for the higher magnification, i.e., there would be less non-uniformity in intensity across the image. Secondly, the resolution which is defined by the radius of the RMS blur circle, as seen on the sky, is better in absolute magnitude for the higher magnification and also falls off more slowly with increasing angle off-axis.

TABLE 2-3

	Off-Axis Angle-Minutes	Area - cm^2 8.3 Å	Area - cm^2 44 Å	Resolution - Arc Seconds RMS Blur Circle Radius
Case 1				
f = 0.75 m	0	2.49	6.56	0
magnification = 4	1	2.23	5.88	0.3
	4	1.48	3.92	4.6
	8	0.67	1.76	17.2
	16	0.33	0.87	70.3
Case 2				
f = 0.50 m	0	1.02	2.85	0
magnification = 6	1	0.95	2.65	0.2
	4	0.71	1.97	3.7
	8	0.40	1.13	13.8
	16	0.18	0.51	57.2

These results are a little arbitrary in the sense that if the element length of the X6 magnifier was increased, it would increase the effec-

tive area and degrade the resolution. Therefore the telescope design can be adjusted to satisfy the requirements of any particular experimenter. Since the higher magnification also provides the larger primary field of view, we have chosen it as our baseline design.

The dimensions and surfaces of the primary and secondary mirrors are defined in Table 2-4 and Figure 2-1. The results of X-ray tracing studies of the resolution as a function of off-axis angle and collecting area are shown in Figure 2-2.

TABLE 2-4

(all dimensions in cms)

Primary Mirror

Focal Length	= 50.0
Principal Radius	= 4.189
Element Length	= 8.378
Grazing Angle	= 1.2°

Surface Equations

Paraboloid $y^2 = d[2\{Z + F + 2a(1 + e)\} + d]$

Hyperboloid $y^2 = (2e + e^2)[\{Z + F + a(1 + e)\}^2 - a^2]$

where
$a = 25.04377$
$d = 0.08754$
$e = 0.00175$

Secondary Mirror

Object Distance	= 23.324
Image Distance	= 139.947
Principal Radius	= 2.034
Element Length	= 5.303

Surface Equations

Hyperboloid #1 $$\frac{(Z + c)^2}{c^2 - b^2} - \frac{y^2}{b^2} = 1$$

Hyperboloid #2 $$\frac{(Z + 2c + f)^2}{F^2 - e^2} - \frac{y^2}{e^2} = 1$$

Where
$b = 0.55498$
$c = 8.35651$
$e = 1.35693$
$f = 49.95470$

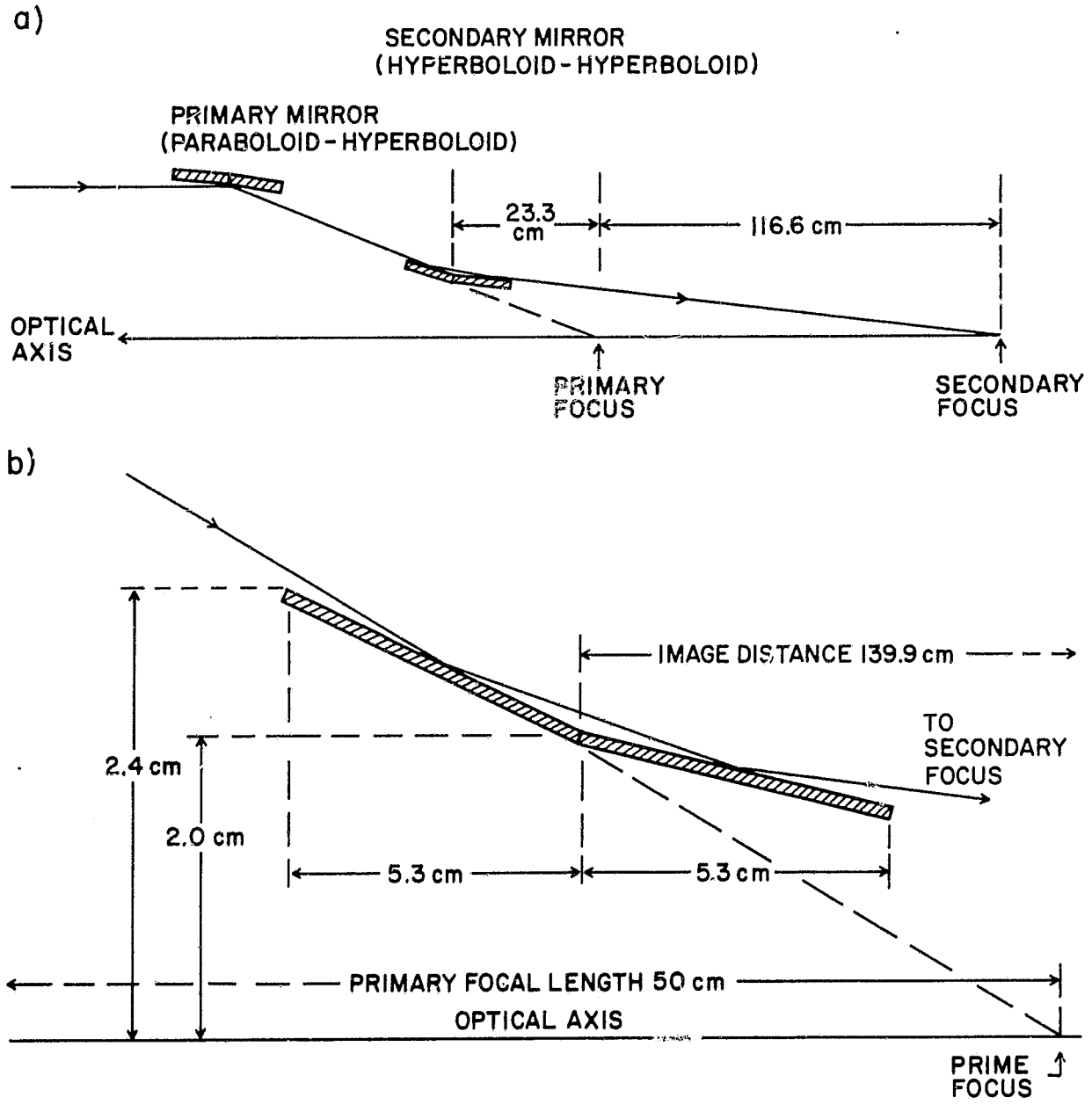

Figure 2-1. Schematic Diagrams of the STARPROBE Mirrors Showing the General Layout (a) and the Dimensions of the Secondary Mirror (b).

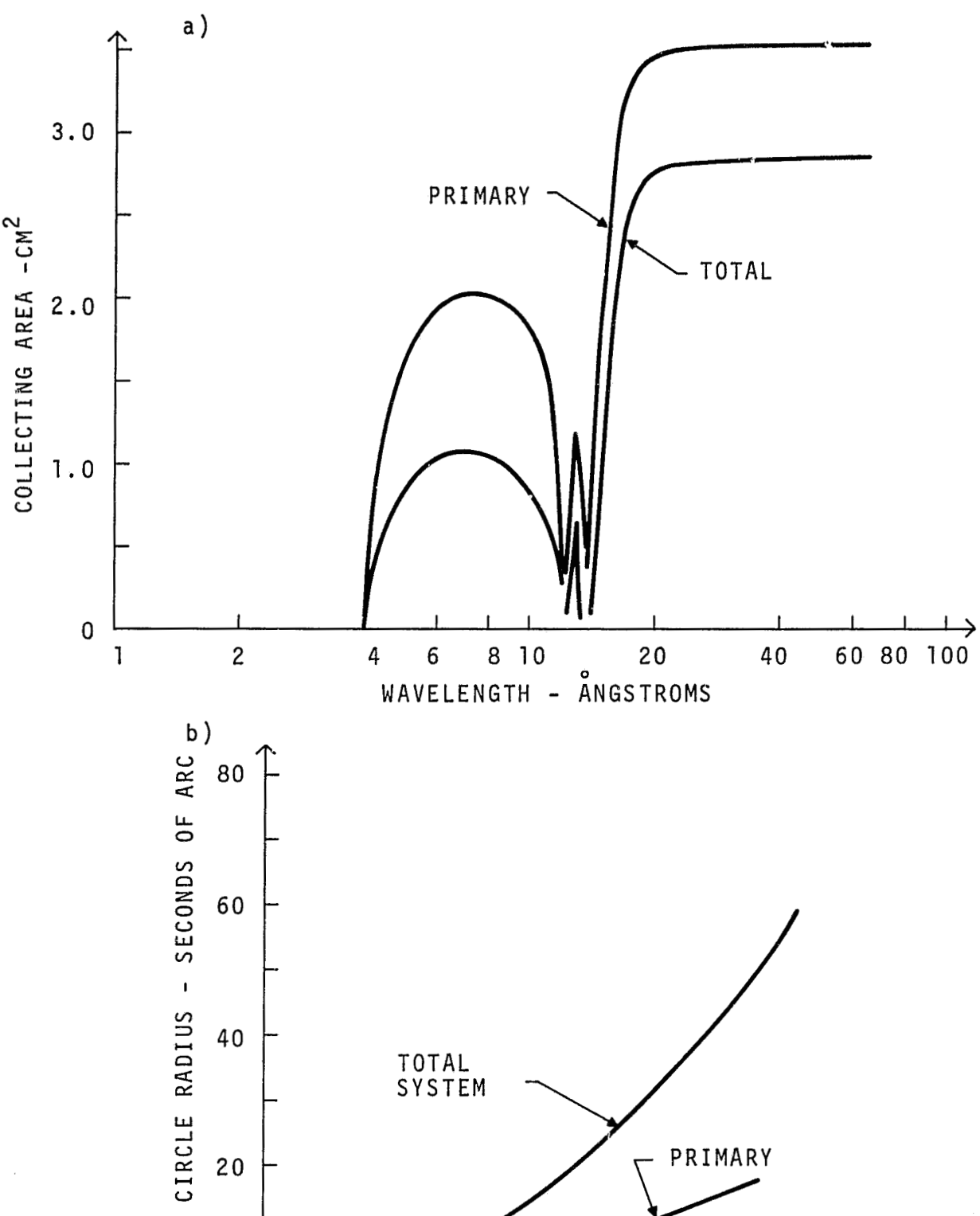

Figure 2-2. Results of the Ray Tracing Studies of the STARPROBE Mirrors. (a) Effective area as a function of wavelength. (b) The variation of the RMS Blur Circle Radius with off-axis angle.

3.0 EXPOSURE TIMES

The focal plane detectors for the STARPROBE X-ray telescope have been baselined as thinned, back-illuminated CCDs with an 800 x 800 array of 15 micron pixels. Such a device does not currently exist but we believe that the natural development of CCD architecture will lead to the development of such devices by the time STARPROBE becomes an approved mission. The following calculations are based on laboratory measurements made on an RCA device with 30 micron pixels at AS&E.[5]

The X-ray flux at the focal plane is given by[6]

$$E_i = \frac{A}{4\pi f^2} \; [EM] \; F_i(T) \text{ ergs cm}^{-2} \text{ sec}^{-1}$$

where A = effective collecting area of telescope,

f = telescope focal length,

$[EM]$ = emission measure,

$F_i(T)$ = spectral integral.

E_i is independent of R, because both the total X-ray flux incident on the CCD and the number of pixels over which it is distributed decrease as R^2. If we take $A = 2.0 \text{ cm}^2$ and $f = 3\text{m}$,

$$E_i = 1.7 \times 10^{-6} \; [EM] \; F_i(t)$$

For a pixel size 15 μm x 15 μm,

$$E_i = 4.3 \times 10^{-12} \; [EM] \; F_i(T) \text{ erg/pixel/sec} \qquad (1)$$

The upper limit for exposure into the CCD without saturation is

$$E_{max} = 1/\bar{\eta}\ [FW] \cdot 3.6 \cdot 1.6 \times 10^{-12}\ \text{erg/pixel}$$

where $\bar{\eta}$ is the average CCD detection efficiency, [FW] is the full well depth in electrons, and $3.6 \times 1.6 \times 10^{-12}$ is the energy in ergs required to produce one electron-hole pair. For a full well depth of 120,000 electrons,

$$E_{max} = 6.9 \times 10^{-7}\ \text{erg/pixel} \qquad (2)$$

It is desirable that exposure not exceed this level anywhere on the CCD, because saturated pixels on RCA CCDs tend to bloom, flooding adjoining pixels.

The lower limit for exposure is based on the CCD system noise, low-level charge transfer efficiency, and/or photon statistics, depending on the scale of spatial variations. This is not likely to be less than $2 \times 10^{-3}\ E_{max}$, as that corresponds to an exposure near 1 keV photon/pixel.

For a typical active region of the corona, we may take[6]

$$[EM] = 2 \times 10^{29}\ \text{cm}^{-3} \quad \text{and} \quad T = 2.5 \times 10^{6}\ ^{\circ}\text{K}$$

For a typical long wavelength filter consisting of 1.1×10^{-4} g cm^{-2} of CH_2 and 6×10^{-5} g cm^{-2} of Aℓ, which corresponds to the thinnest STARPROBE X-ray filter, we take $F_i(T) = 3 \times 10^{-24}$ from Figure 32 of Reference (6). (In this figure $F_i(T)$ is plotted assuming the detector to be film. However, at this temperature the spectral integral for a thinned, back-illuminted CCD should not be very different[7]). Then from Equation (1), we find the exposure to be $E_i = 2.6 \times 10^{-6}$ erg/pixel/sec.

Since the fraction of the radiation at wavelengths shorter than 10 Å is not very large, we expect $\bar{\eta} \gtrsim 0.8$. Thus, from Equation (2) the saturation exposure is at most 8.6×10^{-7} erg/pixel. It would

take only 360 msec for the active region described above to saturate the CCD. This suggests that equivalent exposure times with a thin organic filter should be no more than 100-150 msec.

For the large scale structure described in Reference (6), [EM] = 5 x 10^{27} cm^{-3}, T = 1.6 x 10^6 °K, and $F_i(T) \approx 10^{-24}$ for film so E_i = 2.0 x 10^{-8} erg/pixel/sec. In 150 msec the time-integrated exposure is 6 x 10^{-9} erg/pixel. With $\bar{n}$ near unity, this represents a small (≈ 2) but detectable number of photons per pixel. Bright spots of double this intensity should be distinguishable if they cover several pixels.

For a short wavelength filter, which is typicallly 2.67 mg/cm^2 Be (and which would be one of the thicker STARPROBE filters) the corresponding numbers are F_i = 1 x 10^{-25} and E_i = 8 x 10^{-8} erg/pixel/sec for an active region; if $\bar{n}$ = 2/3, it would take about 13.0 sec to saturate the CCD and a useful exposure would be 5 sec. However, for the large scale features, $F_i \approx 5 \times 10^{-27}$, and $E_i \approx 1 \times 10^{-10}$ erg/pixel/sec, and in 5 sec, the exposure would amount to no more than 1 photon/pixel. Thus, it would be very difficult to record magnified images of the quiet sun because the useful dynamic range of the CCD (three orders of magnitude) is comparable to that of the solar image.

However the principal scientific objectives of the STARPROBE mission, requiring the highest resolution, are the study of active region loops and X-ray bright points, not the quiet coronal structures. In fact the quiet corona would best be studied at the primary focus. A reduction of almost two orders of magnitude in the exposure time would result and the resolution ($\sim$ 100 km) would still be a factor of ten better than can be achieved from earth orbit.

4.0 TELESCOPE PREFILTERS

One of the most critical design choices for the STARPROBE X-ray telescope is the material for the mirror prefilters. The prefilters are mounted directly in front of the telescope aperture and form the primary barrier between the incident solar heat and light flux, which they must reject, while at the same time transmitting the soft X-rays.

Traditionally aluminum films approximately 1500 Å thick mounted on a nickel mesh have been used. They are highly reflective to visible and IR radiation and they can be made relatively pin hole free so that their visible light transmission is on the order of 10^{-3}.

In looking for alternatives we have restricted our choices to metals with lower atomic number and lower density than aluminum. Higher atomic number and higher density metals would require even thinner films than aluminum for satisfactory X-ray transmission. This would present difficulties in terms of structural integrity and heat conduction. The non-metallic elements can, as compounds, be made into films, the hydro- and flurocarbons. However, they are transparent and tend to have low melting points.

The two metals which satisfy the criteria are magnesium and beryllium. However only beryllium is available in sufficiently thin foils; magnesium has the added disadvantages of tarnishing in air and in the form of thin foils has a relatively low ignition temperature.

The X-ray transmission of aluminum and beryllium are compared in Figure 4-1. Both cases consider two prefilters in series. For aluminum our standard specification would provide a total depth of 3000 Å (0.3 microns). The transmission of 6000 Å (0.6 microns) of beryllium over the 2 - 100 Å range is quite similar to the standard aluminum filter with the beryllium having a slightly higher transmission below 45 Å and somewhat lower above. The beryllium Kα edge occurs at 111 Å above which the beryllium prefilter becomes highly transmitting (>50%) again.

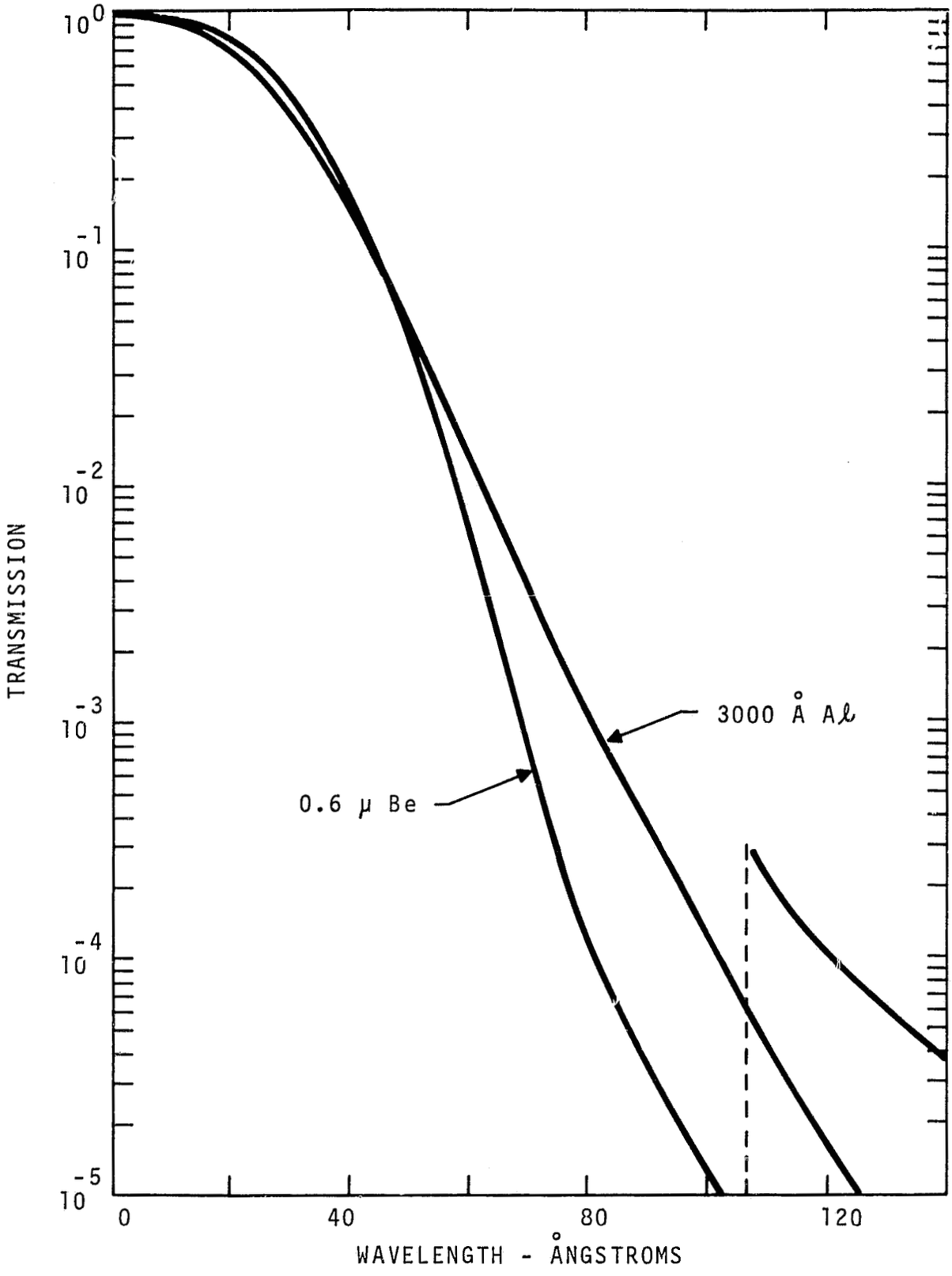

Figure 4-1. A Comparison of the X-Ray Transmission of Aluminum and Beryllium Foils.

which the beryllium prefilter becomes highly transmitting (>50%) again. Beryllium prefilters have two advantages they can be made thicker and hence stronger and the melting point is twice as high as aluminum (1276°C compared to 600°C). The thermal and structural analysis (section 5.4) shows that they have a better safety factor and we have baselined their use.

In practice the first foil of the prefilter might be slightly thinner (2.5 micron) and be coated with a few hundred Angstroms of aluminum to increase its reflectivity.

Beryllium foils are commercially available in thicknesses down to 0.1 microns. For strength the foils would be supported by a mesh which would be epoxy cemented to the foil. In our thermal analysis we have studied silver and copper meshes. Silver, because of its higher conductivity, keeps the films slightly cooler, while copper is slightly stronger. Meshes of either material can be obtained commercially. The epoxy used to attached the film to the mesh is only several hundred Angstroms thick and consequently does not impose a conductive barrier between the film and the mesh. The epoxies are also capable of withstanding the high operating temperatures expected at perihelion.

5.0 STRUCTURAL AND THERMAL ANALYSIS

5.1 Introduction

The design of X-ray telescopes for space applications has been perfected during the last decade and in this regard STARPROBE is a straightforward design task. The condition that makes the STARPROBE design so challenging is the thermal environment. The telescope must look directly at the sun in order to detect the soft X-ray emission and the design task is to shield it from both the direct and indirect thermal radiation.

The configuration of the STARPROBE instrument bay has been taken from the Jet Propulsion Laboratory Science Options Review package dated 1/6/81. Figures 5-1 and 5-2 show the scientific instruments protected from the sun by the primary shield which blocks the direct solar radiation except for a central aperture through which the sun is viewed. Protecting the instruments from the rear of the primary shield are a number of MLI covered secondary shields. In the middle of the central aperture between the secondary shields and the X-ray telescope is a heat rejection mirror. This mirror intercepts all the radiation passing through the central aperture except that in an annulus around the outside of the mirror which strikes the entrance aperture of the telescope. Figure 5-3 is a sketch showing the configuration in the area of the X-ray telescope. The thermal boundary conditions are approximate upper bounds obtained from the JPL model (R. Miyake, private communication).

It has been assumed that STARPROBE will be a shuttle-launched-mission. Therefore the instrument must be able to withstand the shuttle launch acoustic and vibration loads. AS&E's experience with designs for shuttle-launched experiments (e.g., ISPM, AXAF, etc.) has shown the spectra presented in Figure 5-4 for random vibration and Figure 5-5 for acoustic noise to be typical and they have been used in this study.

Starprobe

OPTICAL SPACECRAFT CONFIGURATION
SIDE VIEW

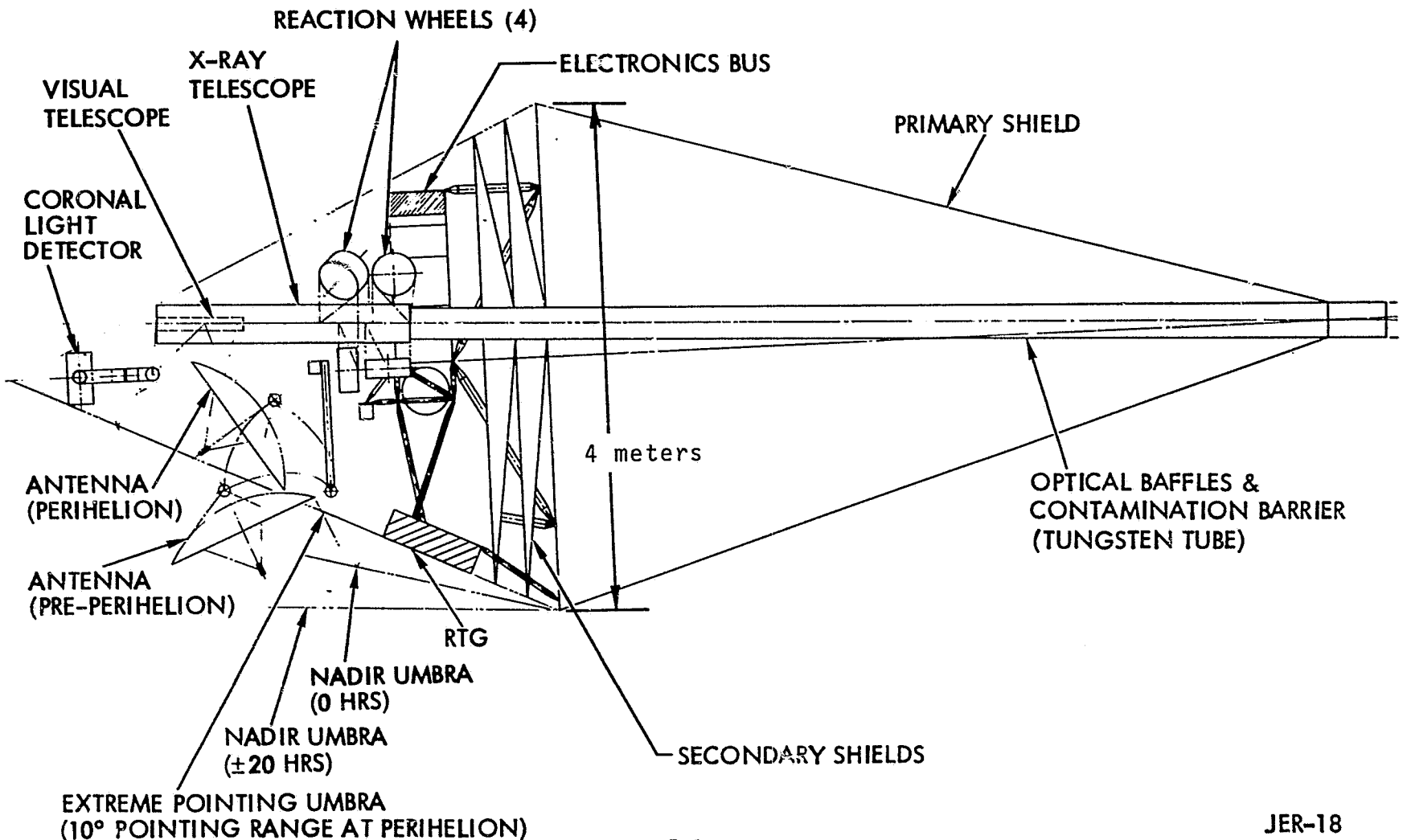

Figure 5-1.

JER-18
1/6/81

FULL SCIENCE SPACECRAFT CONFIGURATION
PERSPECTIVE VIEW

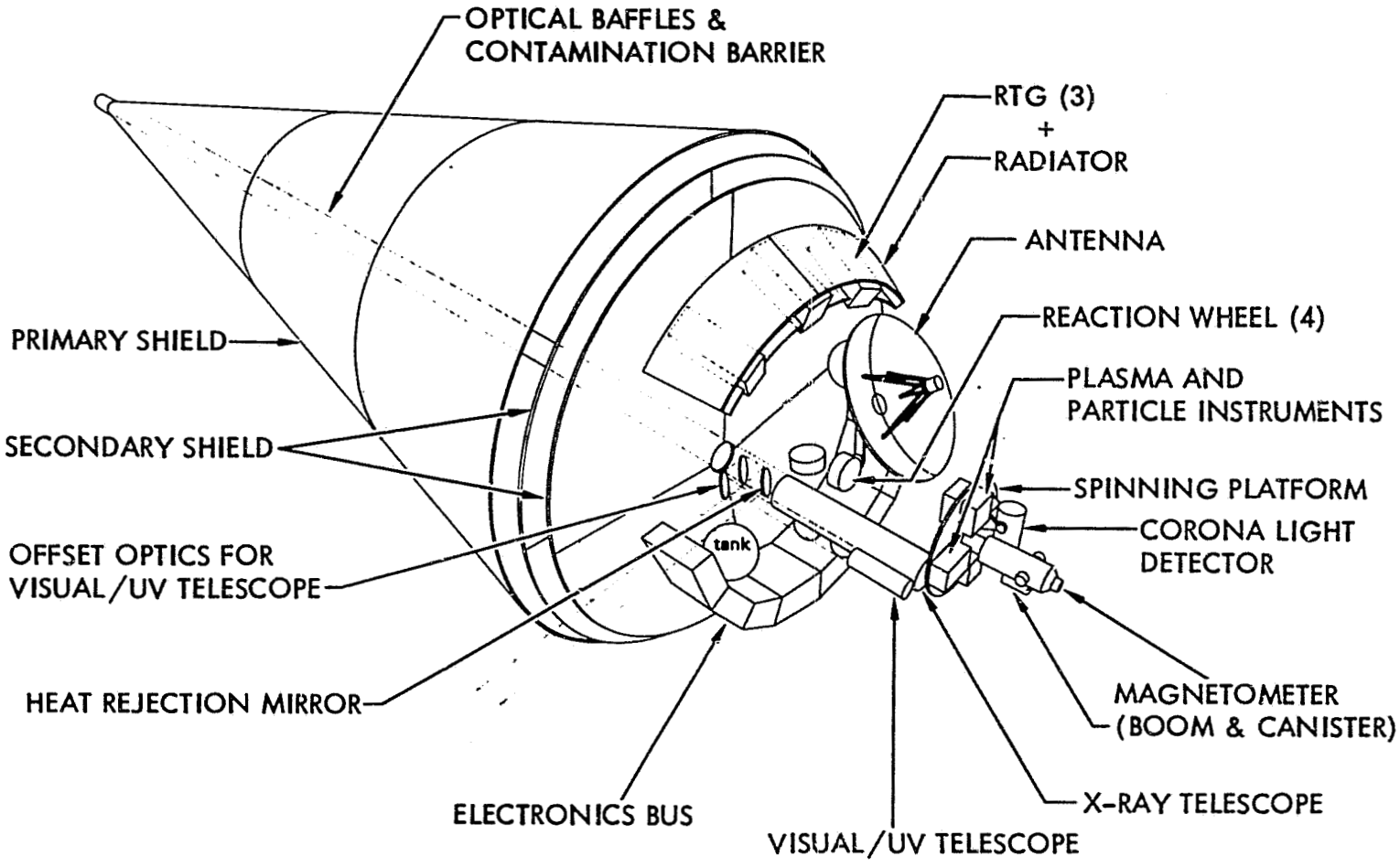

JER-13
1/6/81

Figure 5-2.

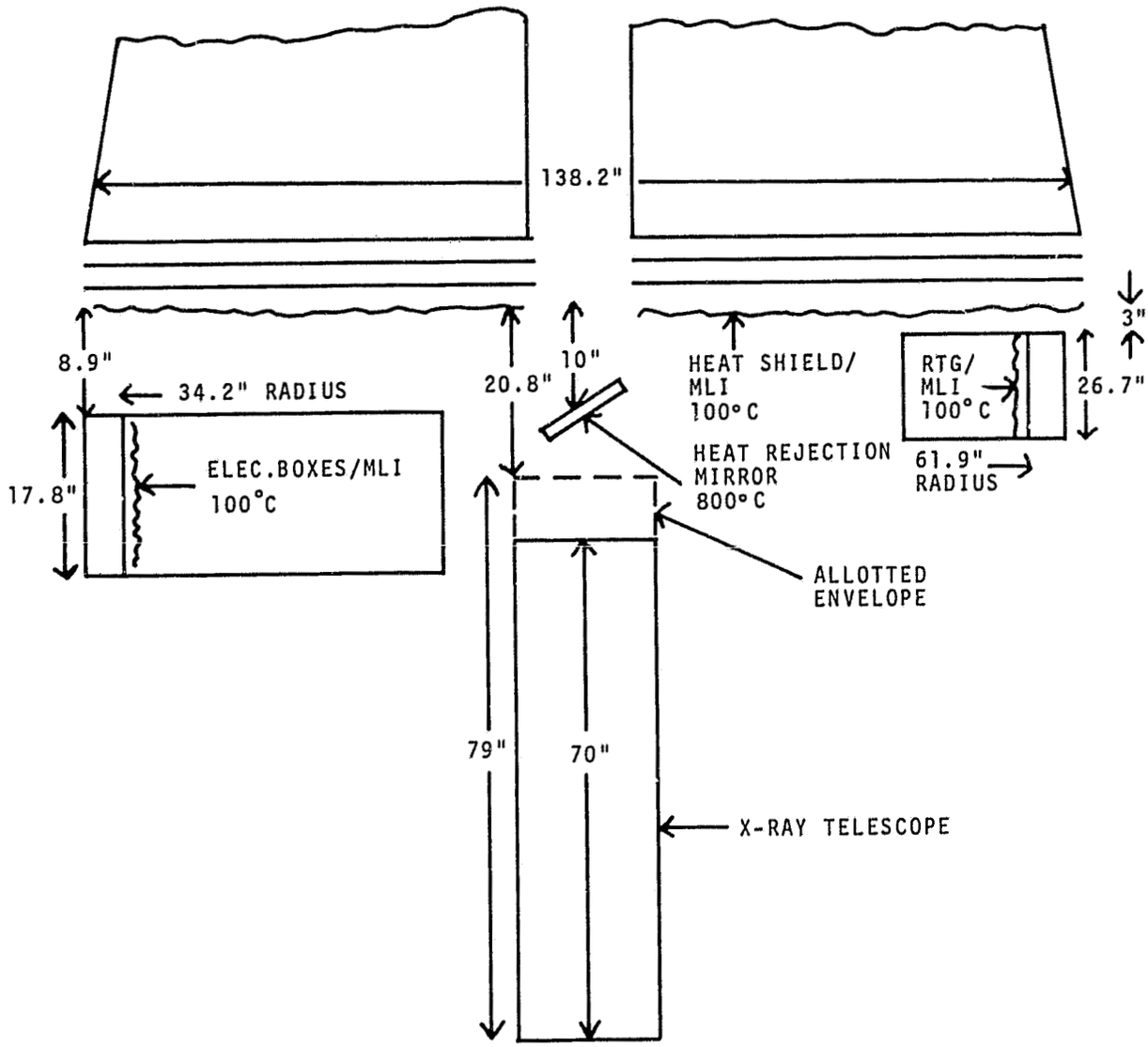

Figure 5-3. Proposed Layout for the STARPROBE X-Ray Imaging Experiment.

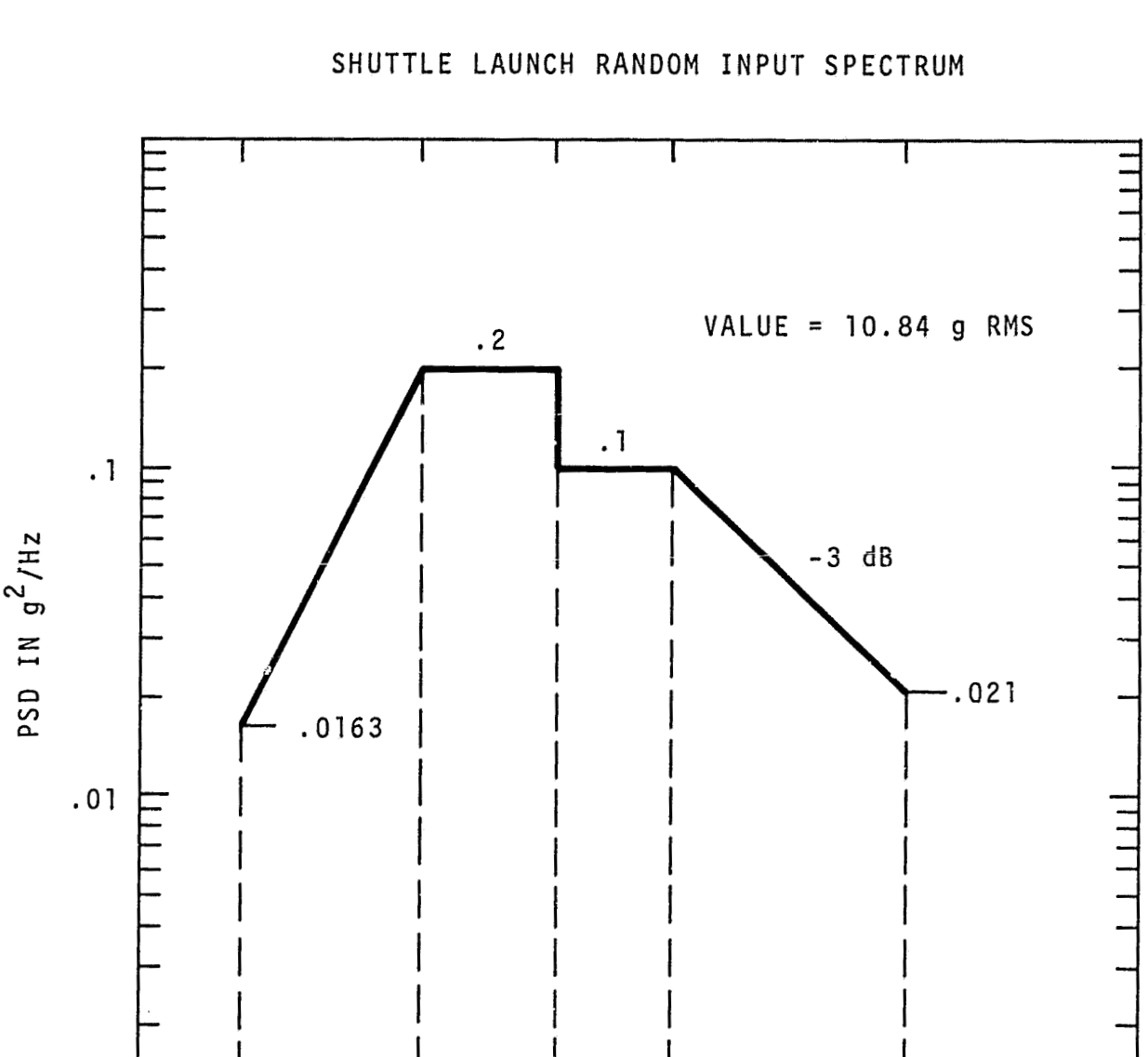
SHUTTLE LAUNCH RANDOM INPUT SPECTRUM
VALUE = 10.84 g RMS
.2
.1
-3 dB
.0163
.021
PSD IN g²/Hz
.1
.01
.001
20
70
180
400
2000
FREQUENCY IN Hz

Figure 5-4.

ISPM ACOUSTIC ENVIRONMENT

1/3 Octave Band Center Frequency (Hz)	1/3 Octave Band Sound Pressure Level (dB)*	
	Flight Level	Qualification Level
31.5	124	128
40	129	133
50	130.5	134.5
63	132	136
80	132.5	136.5
100	133	137
125	133	137
160	133	137
200	133	137
250	133	137
315	132	136
400	131	135
500	129.5	133.5
630	128	132
800	126.5	130.5
1000	125	129
1250	124	128
1600	123	127
2000	122	126
2500	121	125
3150	120	124
4000	118.5	122.5
5000	117	121
6300	115.5	119.5
8000	114	118
10000	112.5	116.5
OVERALL	143.5	147.5

* (dB re 0.0002 μ bar)

Figure 5-5. Acoustic Environment used for the STARPROBE Study.

Four areas have been addressed in this study, namely

1. the selection of materials for the optical bench and the X-ray mirrors,
2. the structural analysis of the optical bench and the mass properties of the instrument,
3. the design of the thermal prefilters to determine survivability to the expected thermal and acoustics loads, and
4. the total instrument's thermal performance.

5.2 Material Selection

The most widely used materials for the fabrication of X-ray mirrors are nickel-coated beryllium and fused silica. The optical bench material must be compatible with the mirror material from the stand point of thermal expansion. Obvious pairings are a beryllium optical bench with a beryllium mirror and a graphite/epoxy bench with a fused silica mirror. (Note. Invar may also be matched to fused silica but because of its high density and hence mass it has not been considered for this application.) With good matches between the CTE's (coefficient of thermal expansion) in both sets, the deciding factor is their susceptibility to thermal gradients. The material's CTE determines how much each set warps under a given gradient condition while their thermal conductivities determine how large a gradient will occur in a given thermal environment. The ratio of the CTE to thermal conductivity for each material indicates how much relative warping might occur and therefore low values of the ratio are preferred.

Fused Silica CTE	$= 0.5 \times 10^{-6}$
Thermal Conductivity	$= 0.8$
Ratio $= 0.5 \times 10^{-6}/0.8$	$= 0.625 \times 10^{-6}$

Graphite Epoxy CTE	$= \pm 0.05 \times 10^{-6}$
Thermal Conductivity	$= 22$
Ratio $= 0.05 \times 10^{-6}/22$	$= 0.0023 \times 10^{-6}$

Beryllium CTE = 6.5×10^{-6}

Thermal Conductivity = 116

Ratio = $6.5 \times 10^{-6}/116 = 0.056 \times 10^{-6}$

From these factors, it can be seen that, although graphite/epoxy is superior to the beryllium for the optical bench, beryllium is ten times better than fused silica for the more distortion-critical mirror material. Therefore we suggest a beryllium mirror, beryllium optical bench for the instrument baseline.

5.3 Instrument Structure and Mass Properties

In order to construct a thermal model of an optical bench for the X-ray telescope, sizes and thicknesses of main members must be known. A first order structural analysis using assumed weights for components was performed establishing practical sizes for the experiment. An approximate weight summary for the X-ray telescope, showing required components, is presented in Table 5-1.

A structural stress summary based on the 70" x 10" x 10" x 0.04" wall beryllium bench described in the weight summary is presented in Table 5-2. The stresses are based on a maximum loading of 60 g's. This load is an approximation of the maximum loading that the instrument will feel during launch based on the random spectrum in Figure 5-4. Due to the random nature of the launch excitation, a 3σ value of the g RMS content of the random spectrum is used and a factor of 2.0 is applied to account for overall system transmissibility.

The allowable stress for the beryllium was limited to the precision elastic limit (1 micro-inch per inch permanent offset). This insures that there will be negligible post-launch residual distortion in the system which would tend to reduce optical performance.

For the purpose of the preliminary analysis, the bench was assumed to be supported at its mid-point. This allows the bench to grow along

TABLE 5-1
WEIGHT SUMMARY

	Item	Comments	Calculated or Assumed Weight lb	kg
1.	Optical Bench, Beryllium	70" x 10" x 10" Box, .04" Walls	7.54	3.42
	30% Contingency	For Bulkheads, Stiffeners, etc.	2.26	1.03
2.	Primary Mirror, Beryllium	3.3" x 6.6" x .125" Wall	0.56	0.25
	30% Contingency	Mounting	0.17	0.08
3.	Secondary Mirror	1.6" x 2.1" x .03" Wall	0.02	0.01
4.	2 Shutter Assemblies @ .6 lb.	Based on ISPM Design	1.20	0.54
	10% Contingency	-	0.12	0.05
5.	2 Filter Assemblies @ .6 lb.	Based on ISPM Design	1.20	0.54
	10% Contingency	-	0.12	0.05
6.	2 CCD Assemblies @ .9 lb.	Based on ISPM Design	1.80	0.82
	10% Contingency	-	0.18	0.08
7.	Electronics Packages	Based on ISPM Design, Conservative	7.00	3.18
8.	2 Radiators @ 2 lb.	12" x 12" x .125" Aluminum	4.00	1.82
	10% Contingency	-	0.40	0.18
9.	Prefilter Assembly	-	2.00	0.91
	10% Contingency	-	0.40	0.18
10.	MLI	Based on ISPM Design	4.00	1.82
	15% Contingency	-	0.60	0.27
11.	Thermal Control	Based on ISPM Design	0.50	0.23
	10% Contingency	-	0.05	0.02
12.	Focal Plane Positioning Mechanism	-	3.00	1.36
	20% Contingency	-	0.60	0.27
13.	Overall Contingency	-	8.6	3.9
		TOTAL	46.3 lb.	21.0 kg.

TABLE 5-2

STRUCTURAL SUMMARY

- Maximum Bending Stress = 3800 psi
- Beryllium Allowable = Precision Elastic Limit = 8000 psi
- Factor of Safety = 2.11

- Maximum Shear Stress = 1570 psi
- Beryllium Allowable = 4800 psi
- Factor of Safety = 3.06

- Fundamental Bending Frequency = 415 cps

the optical axis without inducing thermal discontinuity loads and distortions into the system.

A sketch of a conceptual design for the X-ray telescope is presented in Figure 5-6. This sketch shows two focal planes detectors one of which would be able to move into place when required. When this happens, the secondary mirror would move out of the X-ray path. The bench and both mirrors are wrapped in MLI to control radiatively induced thermal gradients in the mirrors. The mirrors, prefilters, and CCD's are joined to the bench by low conductive mounts.

5.4 Thermal Prefilters

The X-ray mirror and the optical bench are protected from direct solar illumination by the primary heat shield and the MLI covered secondary heat shields. To allow the X-ray mirror to see the sun an aperture must be cut into the heat shields which then act as a pre-collimator limiting the field of view. The X-ray mirror has an annular aperture. A heat rejection mirror is located in the center of the annulus. The annular aperture is covered by the thermal prefilter assembly which must reflect a large fraction of the incoming thermal energy. The rest must be absorbed and dissipated without melting the prefilters while allowing the soft X-rays to pass through to the detector. The assembly must be strong enough to withstand the launch random and acoustic loads.

The prefilter assembly is the most critical design area of the telescope. If the prefilter can be designed to survive the thermal environment of perihelion, the components located behind the prefilters will be subject to a relatively benign environment. To accomplish this we have developed the design presented in Figure 5-7. The first of the three layers in the assembly is a polished heat rejection device made of aluminum. This reflects incoming thermal radiation in the telescope frontal area outside the viewing aperture. The viewing aperture (in the heat rejection device and the two prefilters) is .25"

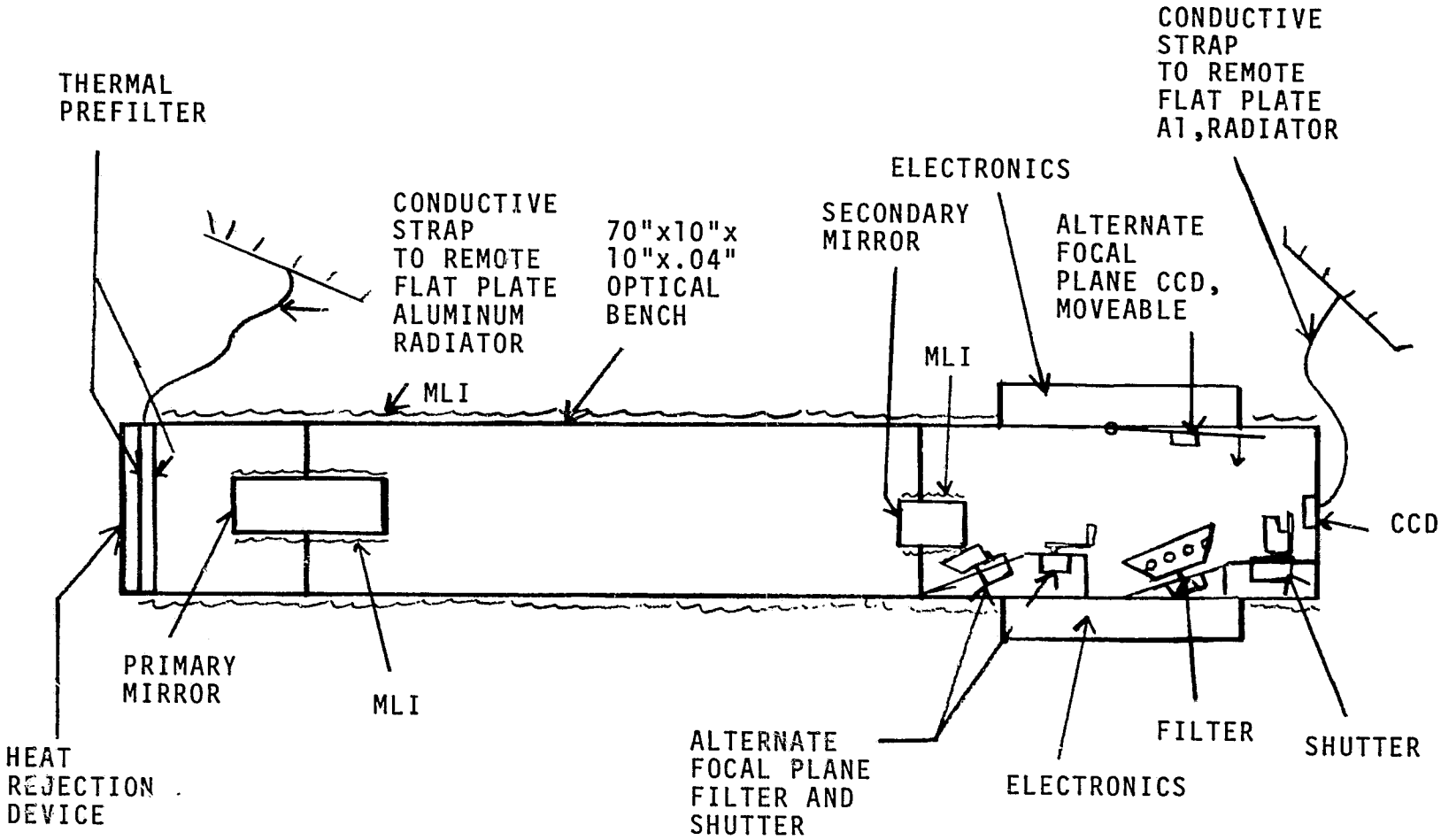

Figure 5-6. Overall Bench.

PREFILTER ASSEMBLY CONCEPT

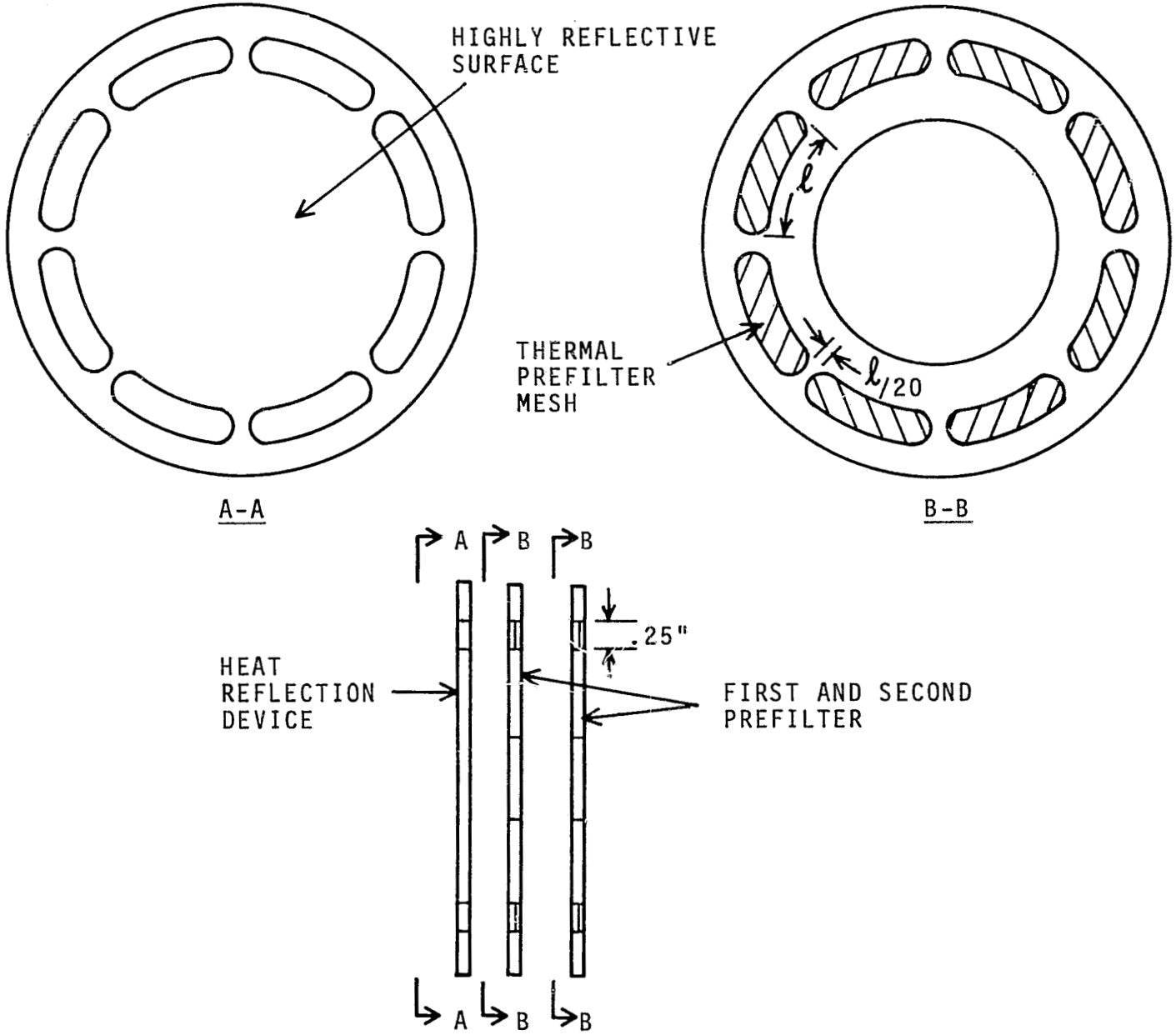

Figure 5-7.

wide. This is determined by the length of the first segment of the primary mirror (3.3") and the grazing angle (1.2°). The annulus must be large enough to allow the entire length of the first segment to receive X-rays. The perfect viewing annulus is given by

$$L = \ell_p \sin \theta$$
$$= 3.3 \sin 1.2°$$
$$= .069"$$

To allow for thermal growth, misalignments and fabrication tolerances an annulus of .25" was used. Two prefilters are used in series to prevent local thermal leakage due to pinholes.

The design of the prefilter is based on providing an open area of 80%. That is the total blockage of the annulus due to the support structure and the wire mesh which supports the prefilter foil must be no more than 20%. Allowing 5% for the supporting structure, the blockage due to the wire mesh is limited to 15%. This limits the mesh wire diameter to 7.5% of the mesh spacing. In the following discussion mesh sizes are defined by the center to center spacing of the individual strands of the mesh.

Preliminary analysis based solely on the incoming solar energy, ignoring radiation from other sources, and on a single mesh cell, showed that the larger the mesh size and the larger the mesh wire, the better conduction to the edge of the filter, but the poorer the conduction from the middle of the mesh cell to the mesh wire. Conversely, the smaller the cell, the better the conduction from the center of the mesh cell to the mesh wire, but the poorer the conduction to the edge of the prefilter due to the smaller mesh wire diameter. The analysis showed an optimum mesh size of 0.052".

Computer models were then generated for different mesh sizes. The sizes used were: 0.0265", 0.0[illegible], 0.0417", 0.0357", 0.0313", 0.025", and 0.005". A thin strip of the first filter was modeled in detail

with the rest of the prefilter treated as a single node or nodes. The second prefilter and the heat rejection device were modeled as single nodes radiatively coupled to the optical bench and conductively coupled to a radiator to deep space which is required to dissipate the heat. Each element of this assembly was radiatively coupled to the surrounding surfaces which acted as sources of radiative heat transfer. Incoming solar radiation was allowed to strike each of the elements of the assembly. These models are shown in Figures 5-8 through 5-12.

The materials considered were aluminum and beryllium for the filter material and silver or copper for the mesh wire. The radiator size and the conduction from the edge of the prefilter assembly to the radiator were varied. The results showed little dependence of the temperature on the radiator size, but a marked dependence on conduction from the prefilter assembly to the radiator. Results for filters of differing mesh sizes are shown in Figure 5-13 through 5-15. Figures 5-13 and 5-14 show the dependence of aluminum and beryllium filters using silver mesh wire on the conduction to the radiator. Data points for copper mesh wire are also shown, displaying a negligible difference in temperature from comparable silver mesh wire data points.

Figure 5-15 shows the dependence of temperature on mesh size. Models were not made for mesh sizes between .005" and .025" so this area of the curves cannot be completed. Based on the aluminum melt temperature of 1680°R, the aluminum has a narrow band of acceptable mesh sizes. Beryllium, with a melt temperature of 2790°R shows a much greater survivable range.

These calculations were performed under the assumption that the first set of beryllium prefilters were covered with aluminum to increase their reflectivity, i.e., the optical properties of aluminum rather than beryllium were used in the calculations. It was pointed out (J. Underwood, Private Communication) that at perihelion either contamination from outgassing of the thermal shields or the direct radiation

0.05" MESH PREFILTER MODEL

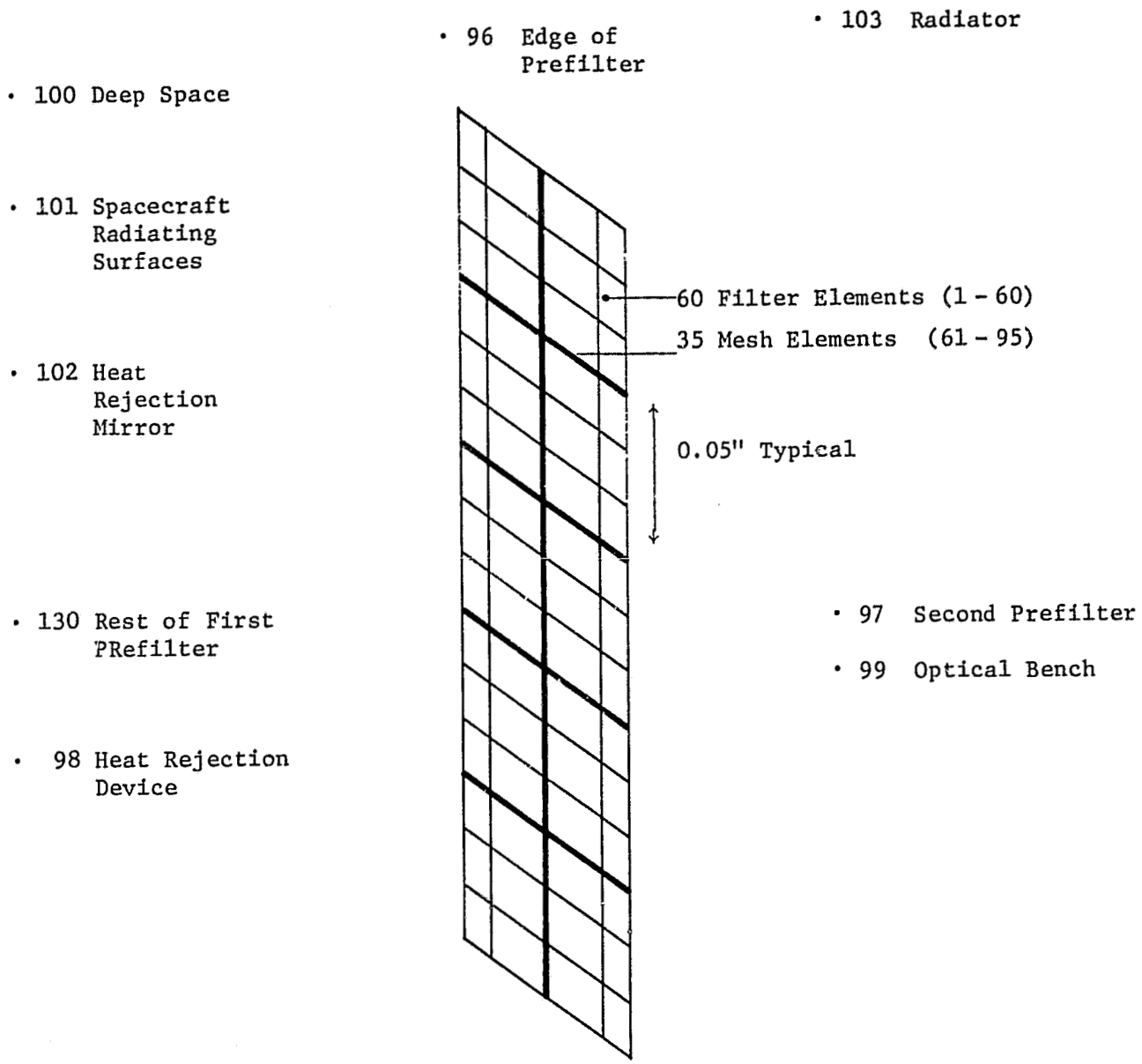

FIGURE 5-8

0.0417" MESH PREFILTER MODEL

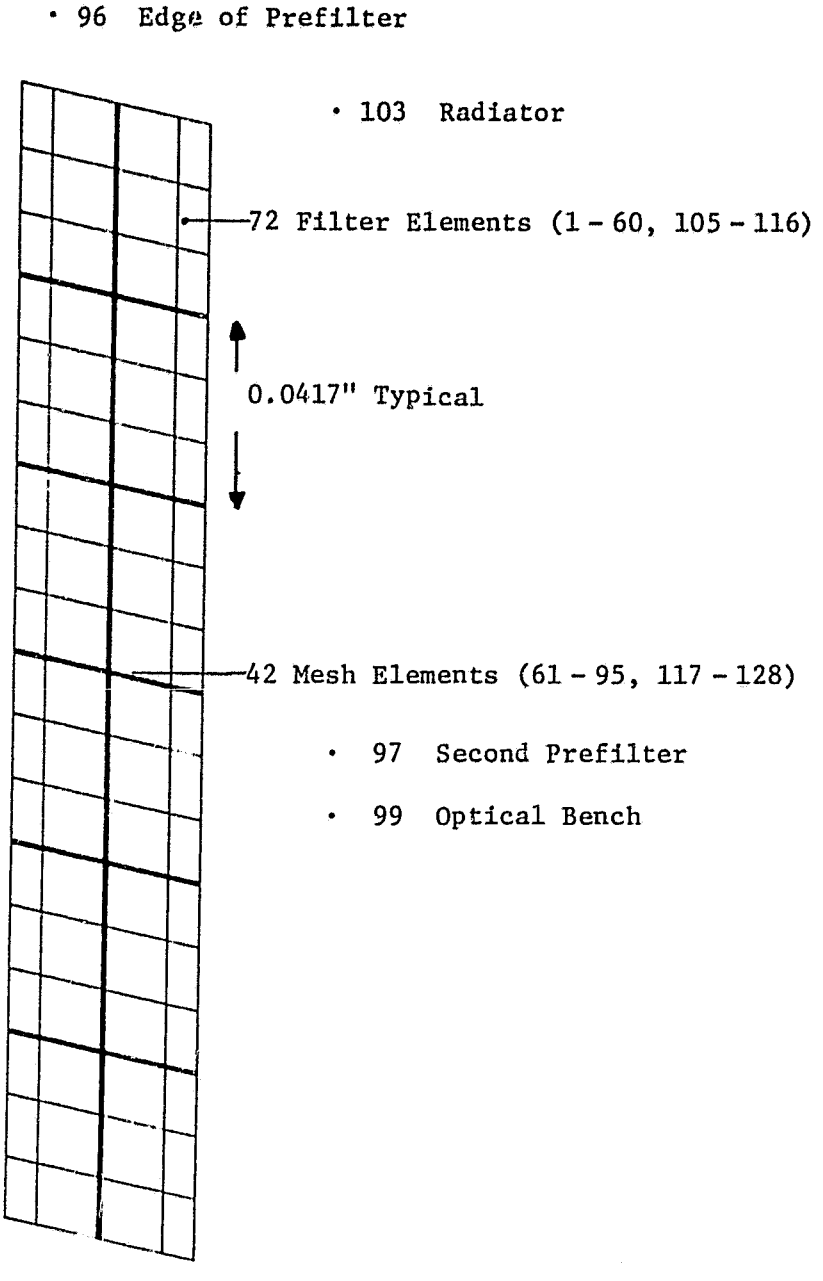

FIGURE 5-9

0.005" MESH PREFILTER MODEL

- 100 Deep Space
- 101 Spacecraft Radiating Surfaces
- 102 Heat Rejection Mirror
- 130 Rest of First Prefilter
- 98 Heat Rejection Device
- 103 Radiator
- 96 Edge of Prefilter

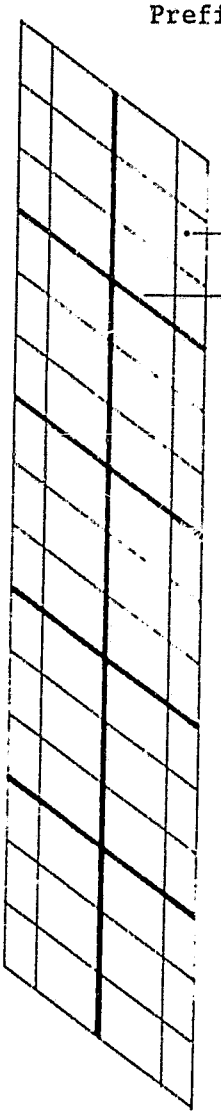

- 97 Second Prefilter
- 99 Optical Bench

109
110
111
112
113
114
115
116
117

Single nodes representing 0.025" x 0.005" segments of first prefilter

FIGURE 5-10

0.0625" MESH PREFILTER MODEL

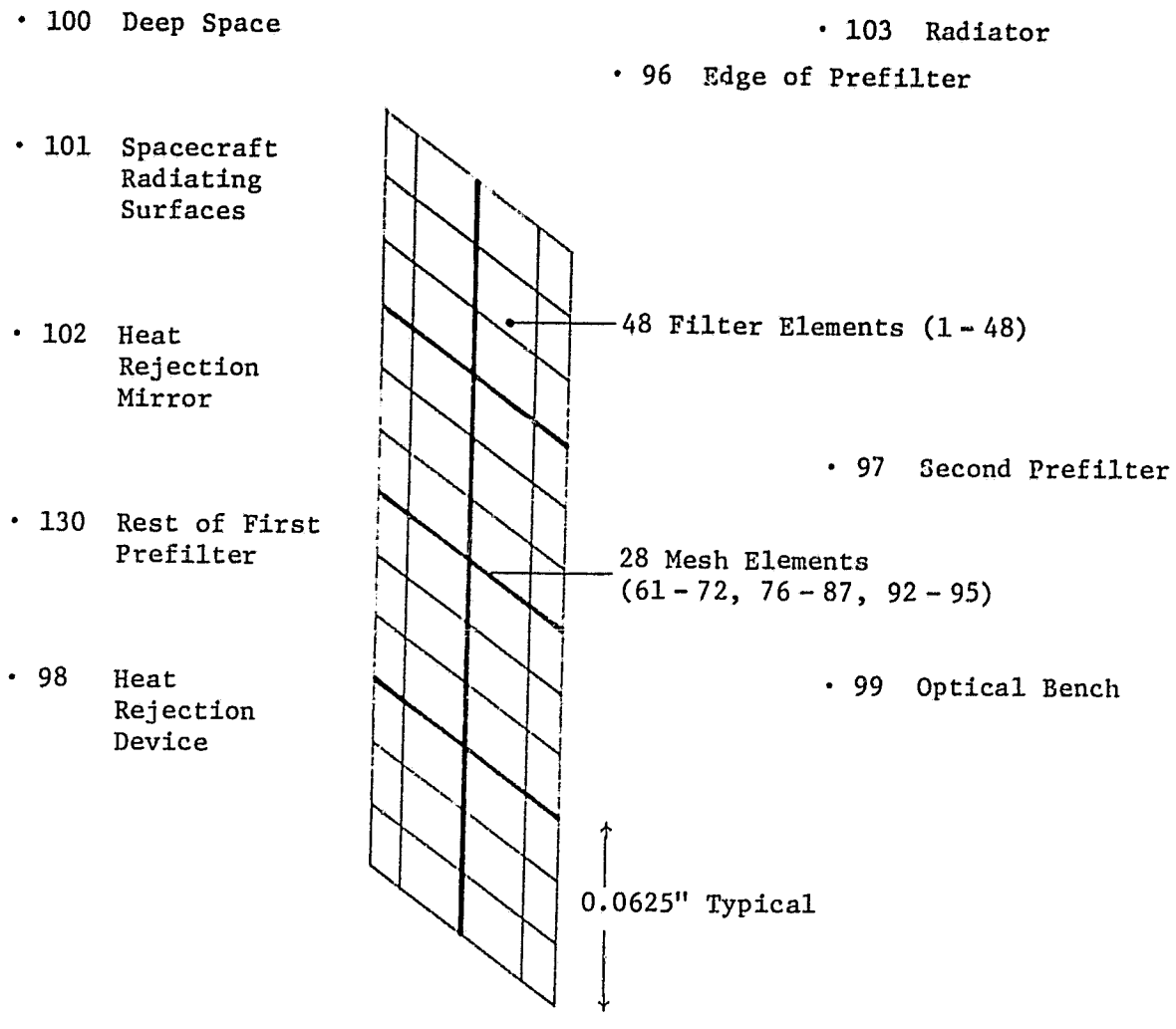

FIGURE 5-11

0.025", 0.0313", and 0.0357" MESH PREFILTER MODELS

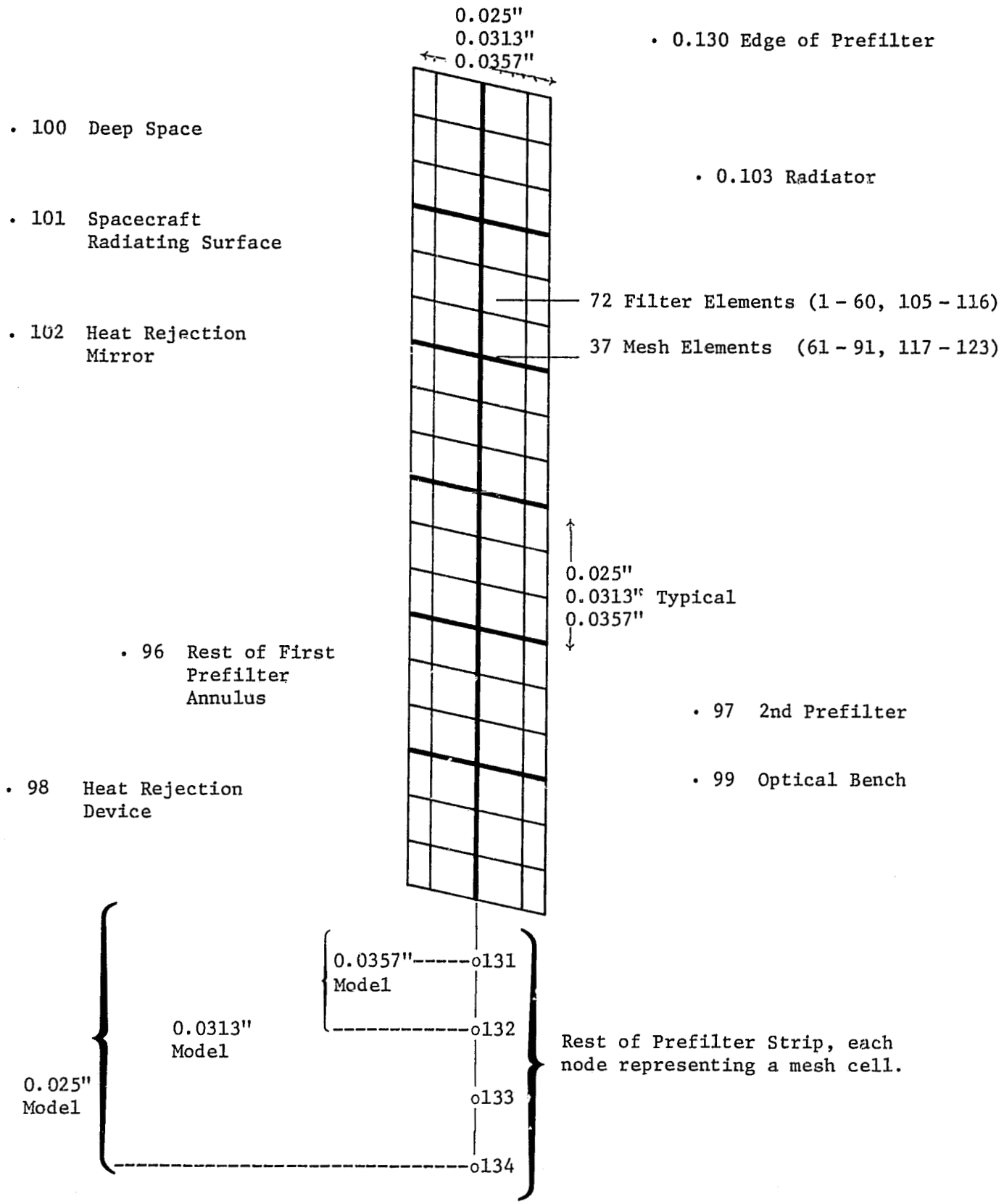

FIGURE 5-12

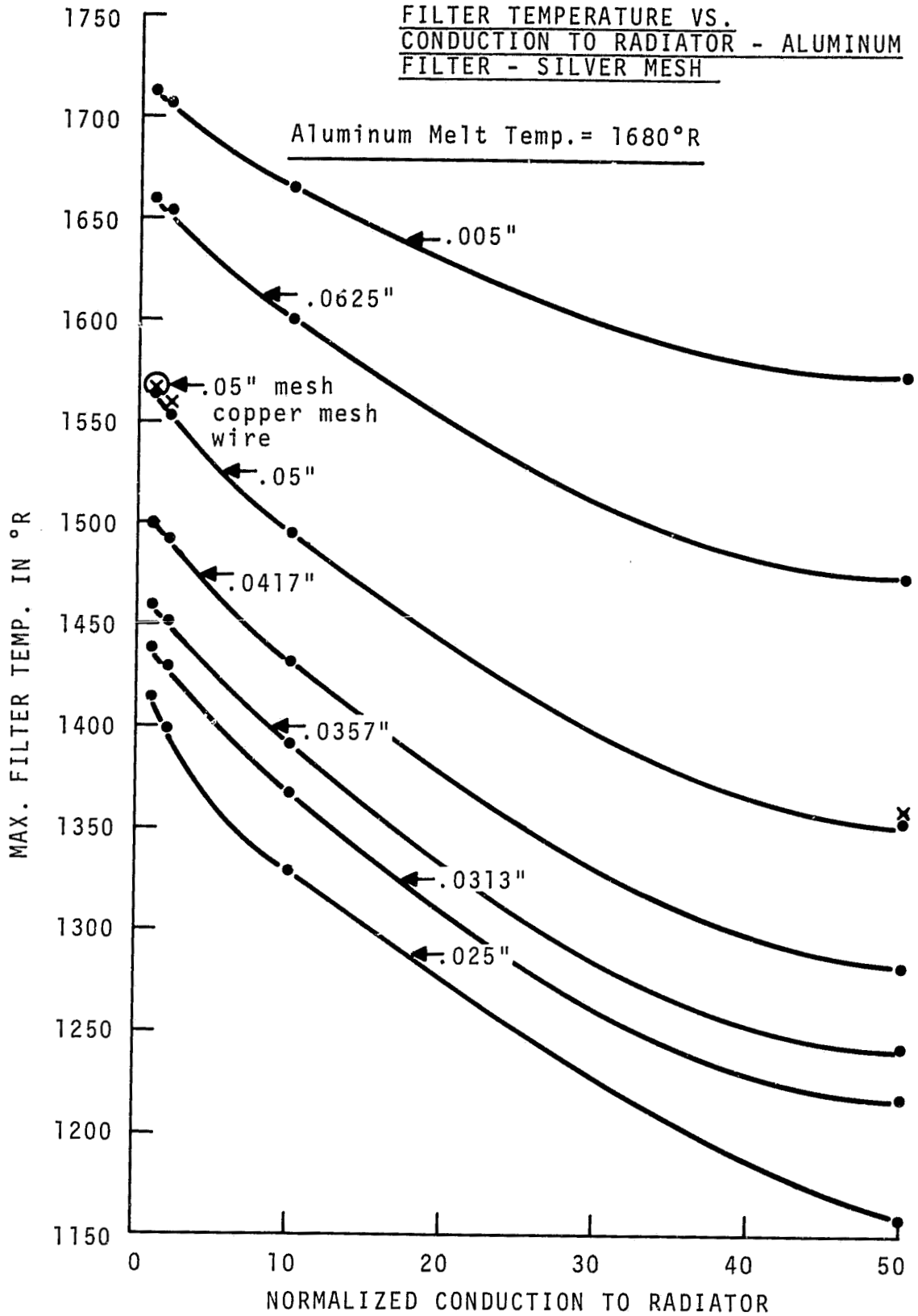
FILTER TEMPERATURE VS. CONDUCTION TO RADIATOR - ALUMINUM FILTER - SILVER MESH
Aluminum Melt Temp.= 1680°R
.005"
.0625"
.05" mesh copper mesh wire
.05"
.0417"
.0357"
.0313"
.025"
MAX. FILTER TEMP. IN °R
1750
1700
1650
1600
1550
1500
1450
1400
1350
1300
1250
1200
1150
0
10
20
30
40
50
NORMALIZED CONDUCTION TO RADIATOR

Figure 5-13.

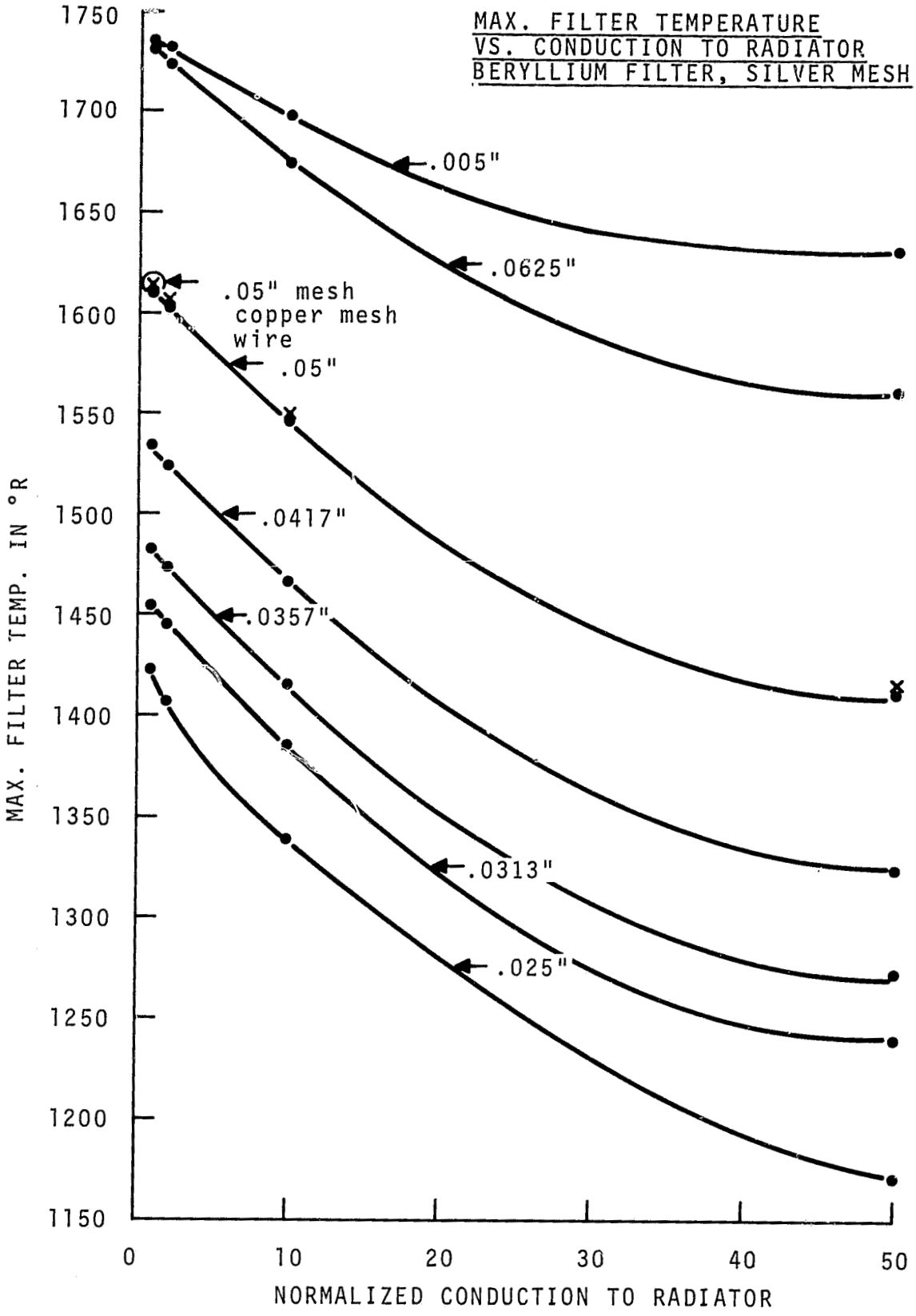
MAX. FILTER TEMPERATURE
VS. CONDUCTION TO RADIATOR
BERYLLIUM FILTER, SILVER MESH
.005"
.0625"
.05" mesh
copper mesh
wire
.05"
.0417"
.0357"
.0313"
.025"
MAX. FILTER TEMP. IN °R
1750
1700
1650
1600
1550
1500
1450
1400
1350
1300
1250
1200
1150
0
10
20
30
40
50
NORMALIZED CONDUCTION TO RADIATOR

Figure 5-14.

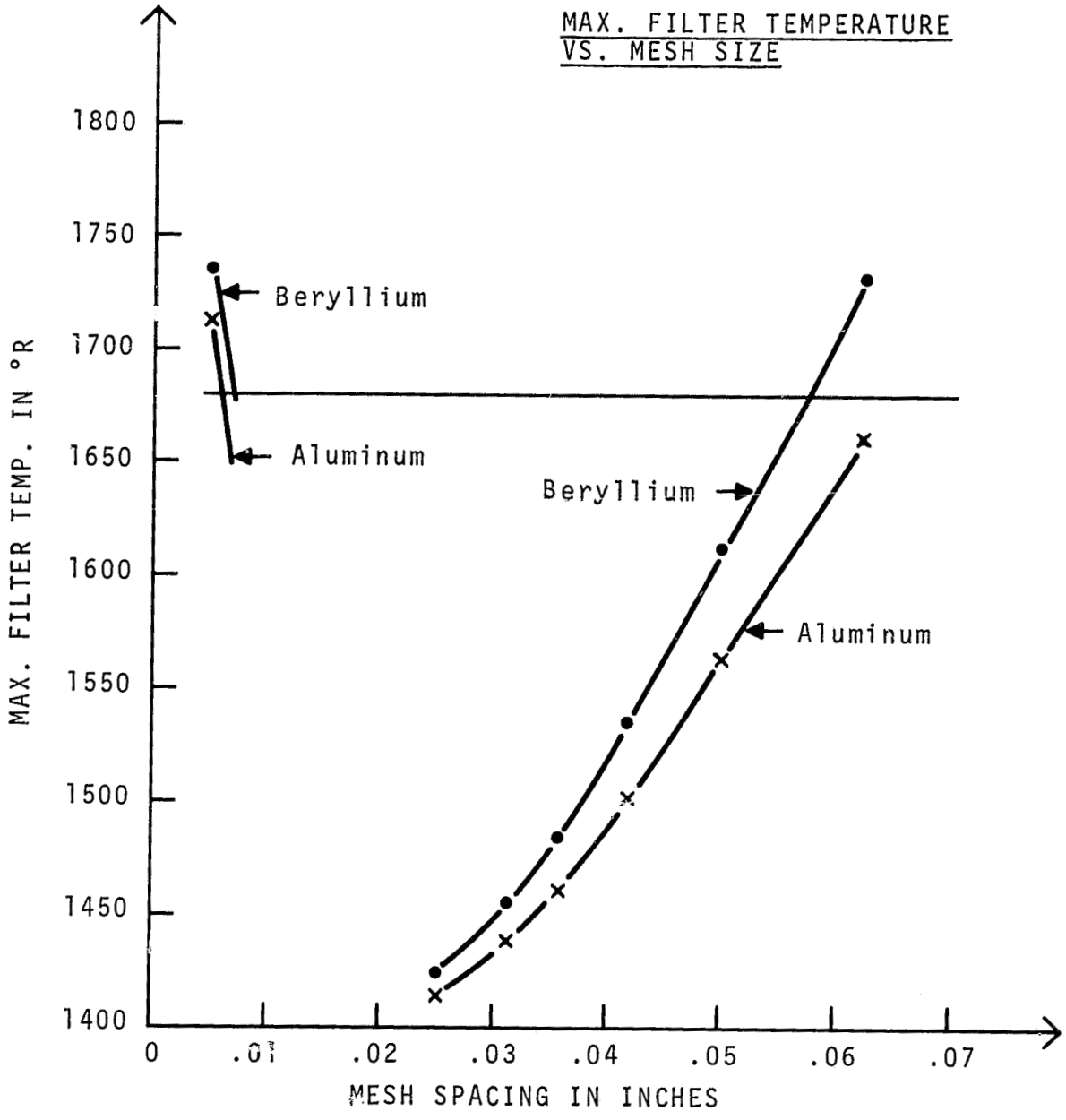
MAX. FILTER TEMPERATURE
VS. MESH SIZE
MAX. FILTER TEMP. IN °R
1800
1750
1700
1650
1600
1550
1500
1450
1400
Beryllium
Aluminum
Beryllium
Aluminum
0
.01
.02
.03
.04
.05
.06
.07
MESH SPACING IN INCHES

Figure 5-15.

effects might degrade the film lowering its reflectivity and hence leading to failure of the prefilter. Consequently we have studied the effect on the prefilter temperature of varying the absorption of the prefilter from 15%, the value with the aluminum coating, to 100%. The optimum silver mesh size was used (0.025") and the increase in absorbtivity caused an increase in radiation heat transfer and absorbed solar heat. The results of the analysis are shown in Figure 5-16. They show that even at the worst case, where all the incident heat is absorbed, the maximum filter temperature is 721°C (1790°R) while the beryllium melting point occurs at 1280°C (2790°R). The maximum mesh temperature is 638°C (1641°R) which is also comfortably below the silver melting point of 960°C (2220°R). The pure aluminum prefilter would not survive under these conditions.

Thus even under a worst case contamination, the beryllium would still function effectively, protecting the X-ray telescope from excessive heat loadings.

5.4.1 Acoustic Performance

A structural analysis of the prefilters based on the acoustic spectrum in Figure 5-5 was carried out to determine the survivability of the prefilters during launch. The qualification overall acoustic pressure level of 147.5 db converts to a static pressure differential of .0688 psi across the filter.

Two modes of failure were investigated, one-time loading and fatigue loading. Due to the random nature of structural response to acoustic vibration, a 3σ level of the static pressure was assumed. In order to survive, the filter material must have an ultimate tensile stress less than this level. Since the loading is also periodic, alternating from $\sigma = 0$ to $\sigma = \sigma_{max}$, a fatigue condition was analyzed. In order to survive the fatigue loading, the material must have an endurance limit less than $1/2\ \sigma_{max}$.

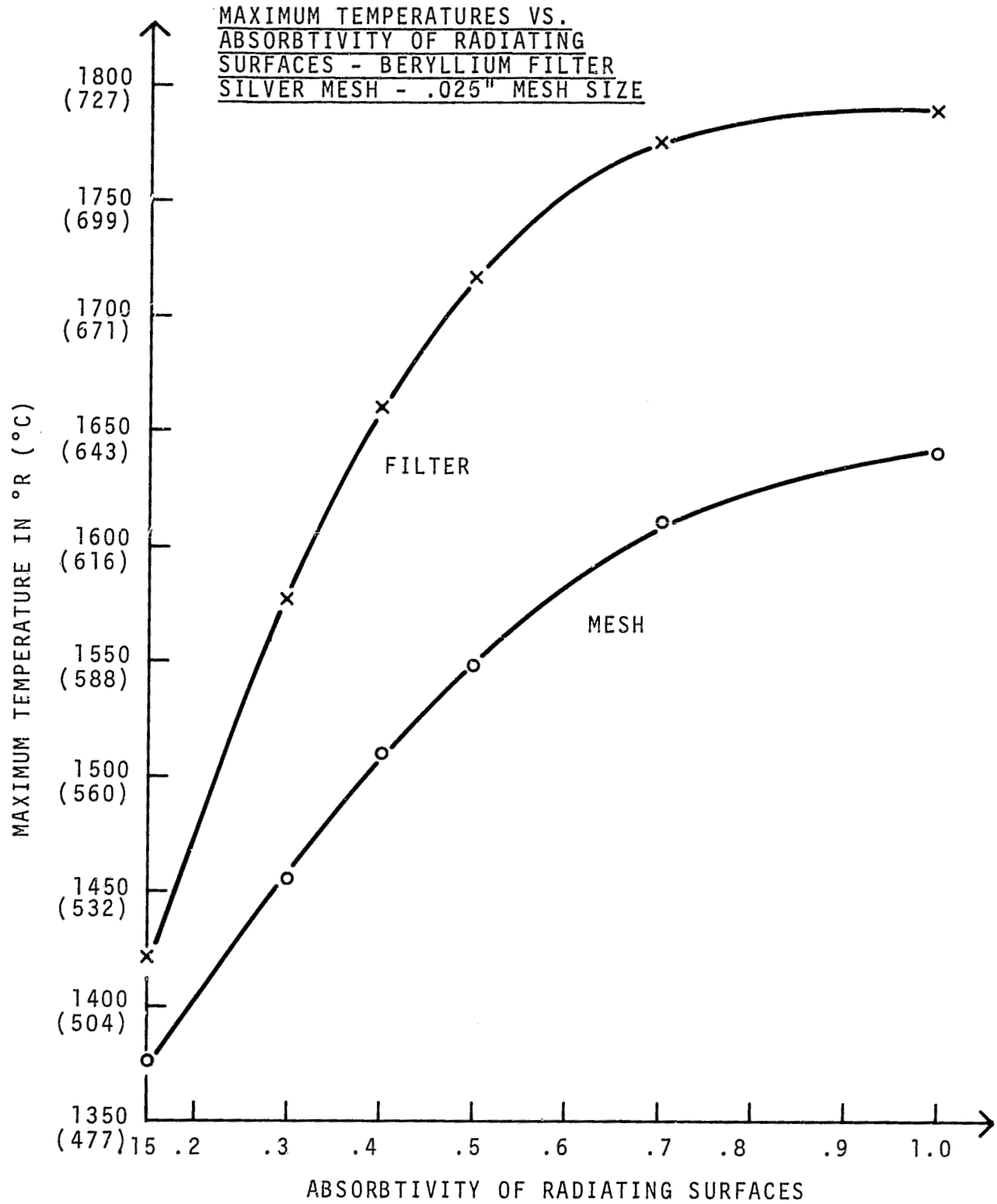
MAXIMUM TEMPERATURES VS.
ABSORBTIVITY OF RADIATING
SURFACES - BERYLLIUM FILTER
SILVER MESH - .025" MESH SIZE
MAXIMUM TEMPERATURE IN °R (°C)
1800 (727)
1750 (699)
1700 (671)
1650 (643)
1600 (616)
1550 (588)
1500 (560)
1450 (532)
1400 (504)
1350 (477)
FILTER
MESH
.15
.2
.3
.4
.5
.6
.7
.8
.9
1.0
ABSORBTIVITY OF RADIATING SURFACES

Figure 5-16.

Two areas of the prefilter were examined for failure. The first was the local stress in the individual filter mesh cell, considering the filter material to be supported on four sides by the mesh wire. The second was the overall stress in the prefilter, looking at the entire prefilter supported by the holder.

Results of these analyses are shown in Figure 5-17 through 5-21. These figures show that the aluminum mesh size must be between .011" and .029" in order to survive launch, while the beryllium filter survives throughout the range we have analyzed. Based on this analysis and review of the allowable stresses (see Appendix) the beryllium filter appears to be a superior candidate from the standpoint of surviving launch.

5.5 Overall System Performance

A thermal model of the overall system was developed and is shown in Figure 5-22. Heat from all radiative and solar sources was considered, including an estimated 2.3 watts for the electronics. Various amounts of heat from supplementary heaters was added to minimize and control gradients in the mirror and bench. Results using 1 ft^2 radiators for the prefilters and for the CCD's are given in Table 5-3 for various heater inputs.

The different heater inputs are used to investigate the reduction of gradients within each mirror and between the primary and secondary mirrors while maintaining the CCD temperature at a reasonable value. Although some smoothing of gradients is achieved by increasing the heater power, the effects are small and the subsequent analysis is based on the thermal environment developed for Q = 2.34 watts.

The distortions in the mirrors and the resulting degradation in resolution of the telescope due to thermal soaks and thermal gradients in the mirrors have been estimated. In order to minimize the problems

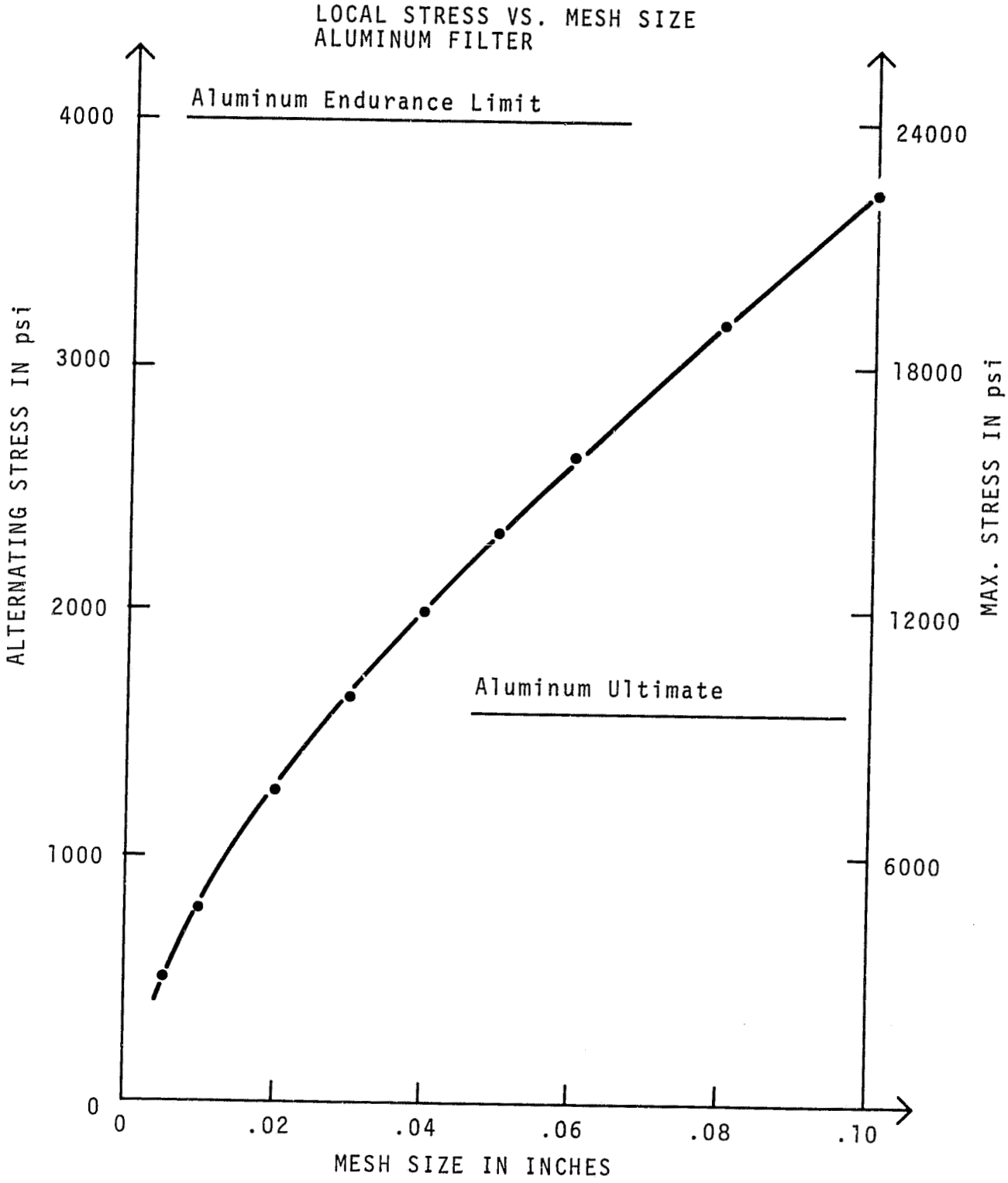
LOCAL STRESS VS. MESH SIZE
ALUMINUM FILTER
Aluminum Endurance Limit
Aluminum Ultimate
ALTERNATING STRESS IN psi
MAX. STRESS IN psi
4000
3000
2000
1000
0
24000
18000
12000
6000
0
.02
.04
.06
.08
.10
MESH SIZE IN INCHES

Figure 5-17.

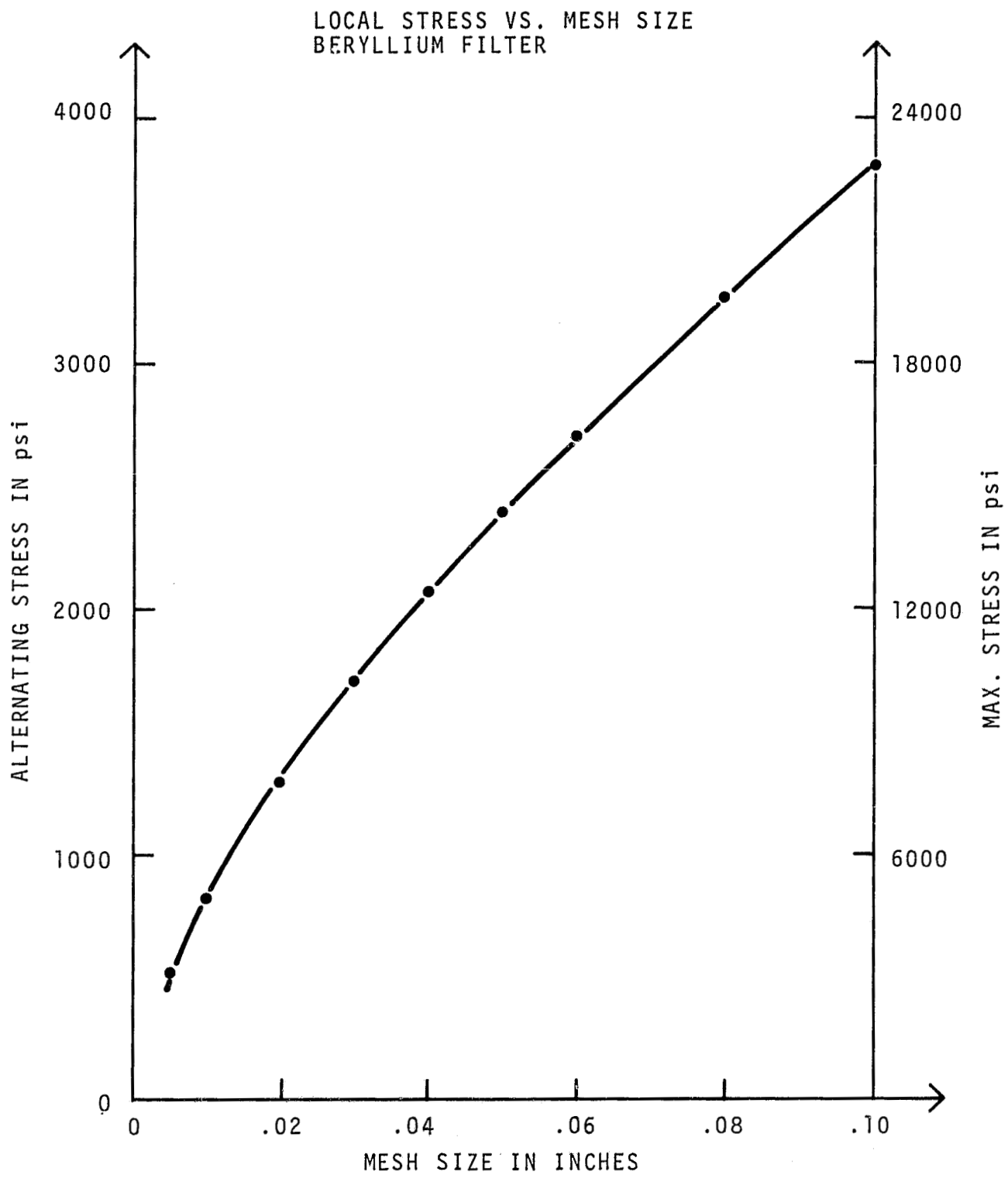
LOCAL STRESS VS. MESH SIZE
BERYLLIUM FILTER
ALTERNATING STRESS IN psi
MAX. STRESS IN psi
4000
3000
2000
1000
0
24000
18000
12000
6000
0
.02
.04
.06
.08
.10
MESH SIZE IN INCHES

Figure 5-18.

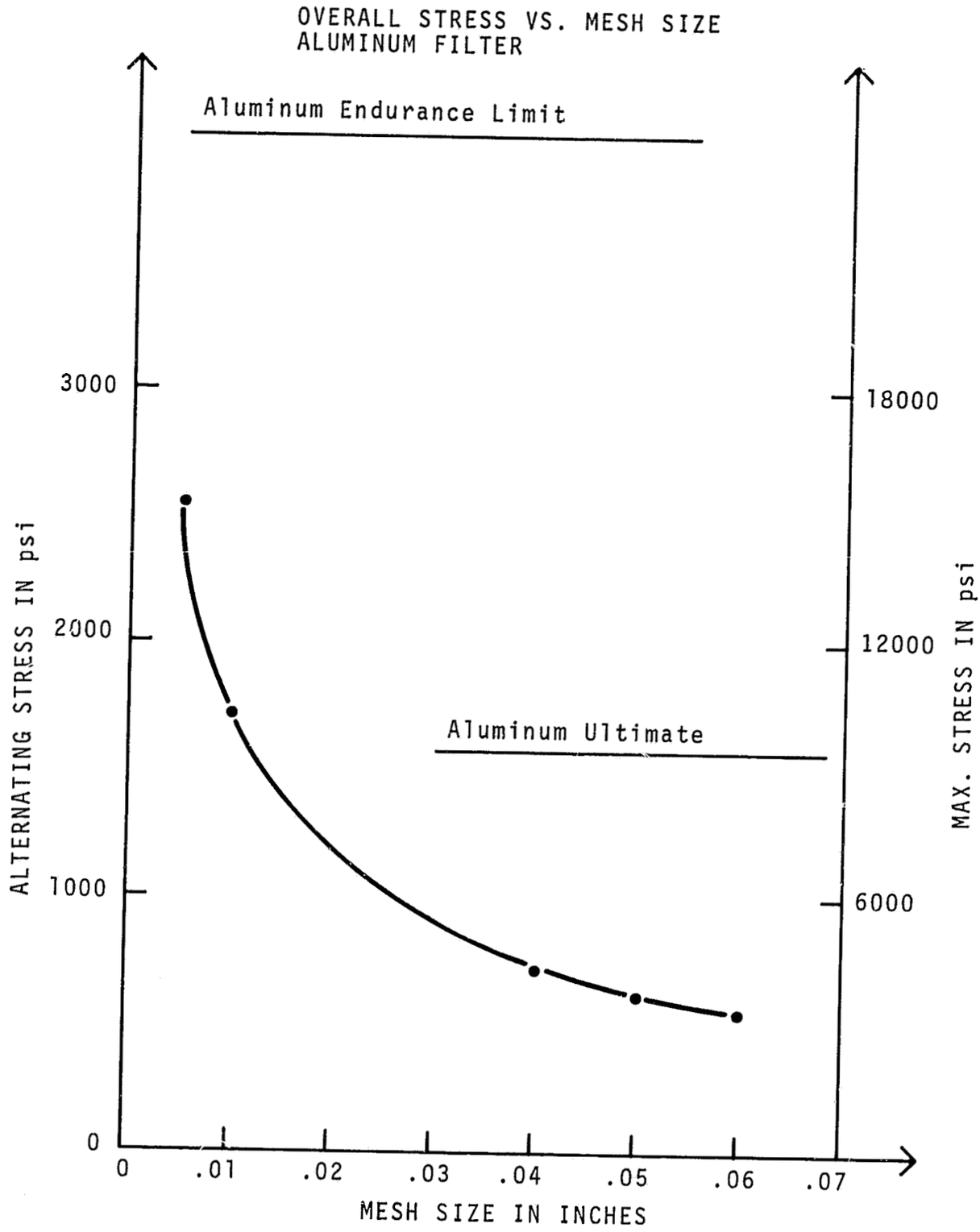
OVERALL STRESS VS. MESH SIZE
ALUMINUM FILTER
Aluminum Endurance Limit
Aluminum Ultimate
ALTERNATING STRESS IN psi
MAX. STRESS IN psi
3000
2000
1000
0
18000
12000
6000
0
.01
.02
.03
.04
.05
.06
.07
MESH SIZE IN INCHES

Figure 5-19.

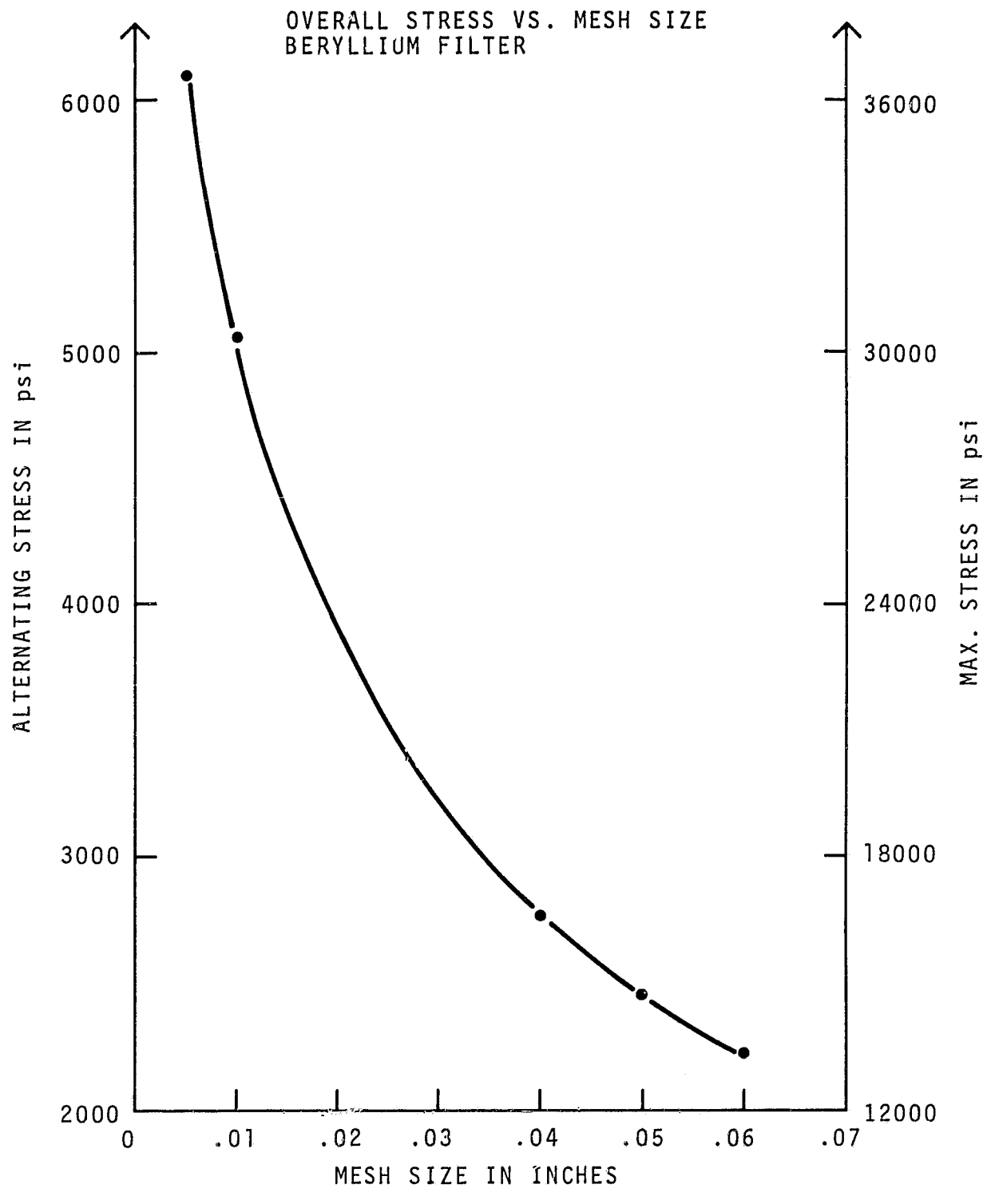
OVERALL STRESS VS. MESH SIZE
BERYLLIUM FILTER
ALTERNATING STRESS IN psi
MAX. STRESS IN psi
6000
5000
4000
3000
2000
36000
30000
24000
18000
12000
0
.01
.02
.03
.04
.05
.06
.07
MESH SIZE IN INCHES

Figure 5-20

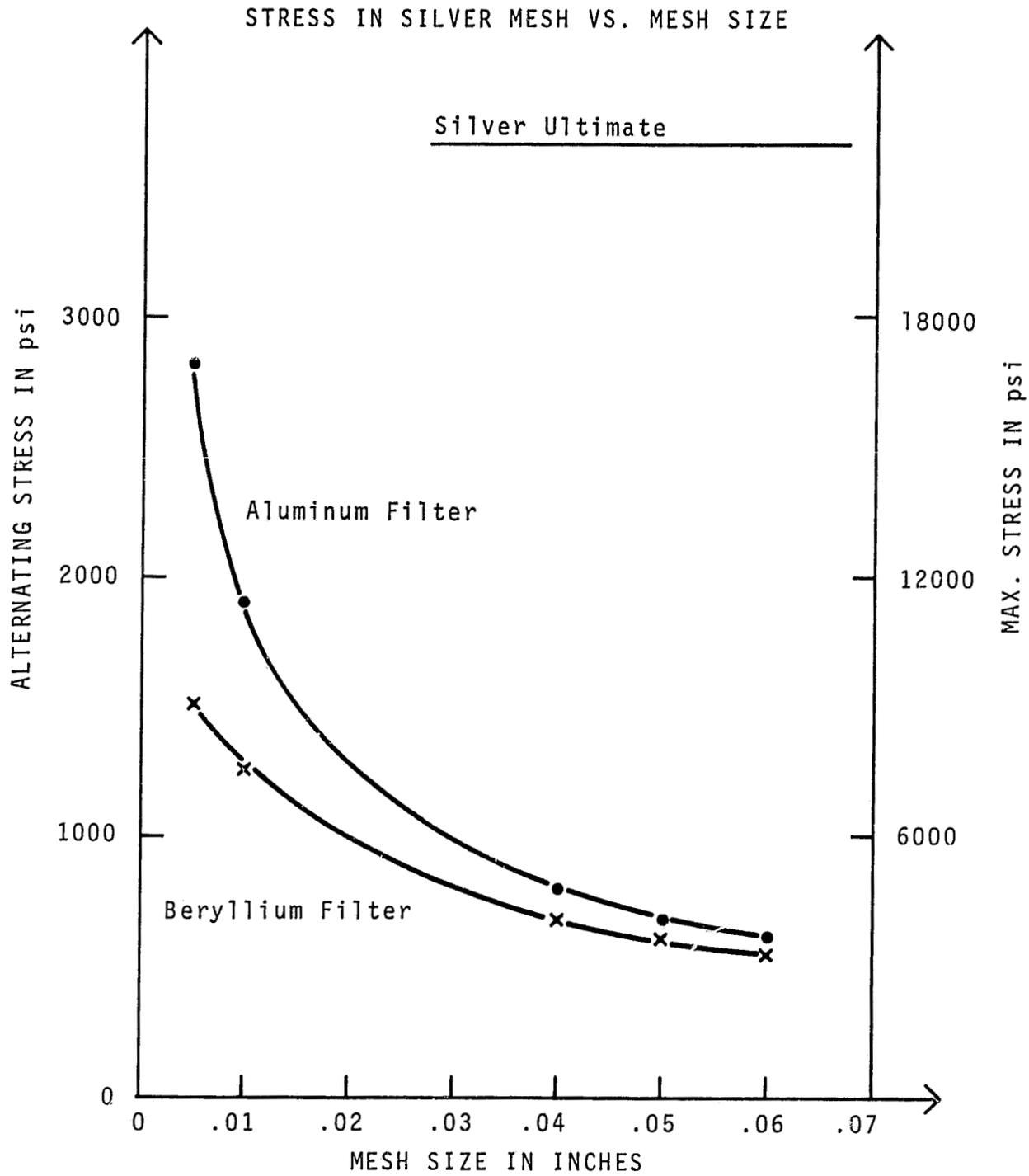
STRESS IN SILVER MESH VS. MESH SIZE
Silver Ultimate
ALTERNATING STRESS IN psi
MAX. STRESS IN psi
3000
2000
1000
0
18000
12000
6000
Aluminum Filter
Beryllium Filter
0
.01
.02
.03
.04
.05
.06
.07
MESH SIZE IN INCHES

Figure 5-21

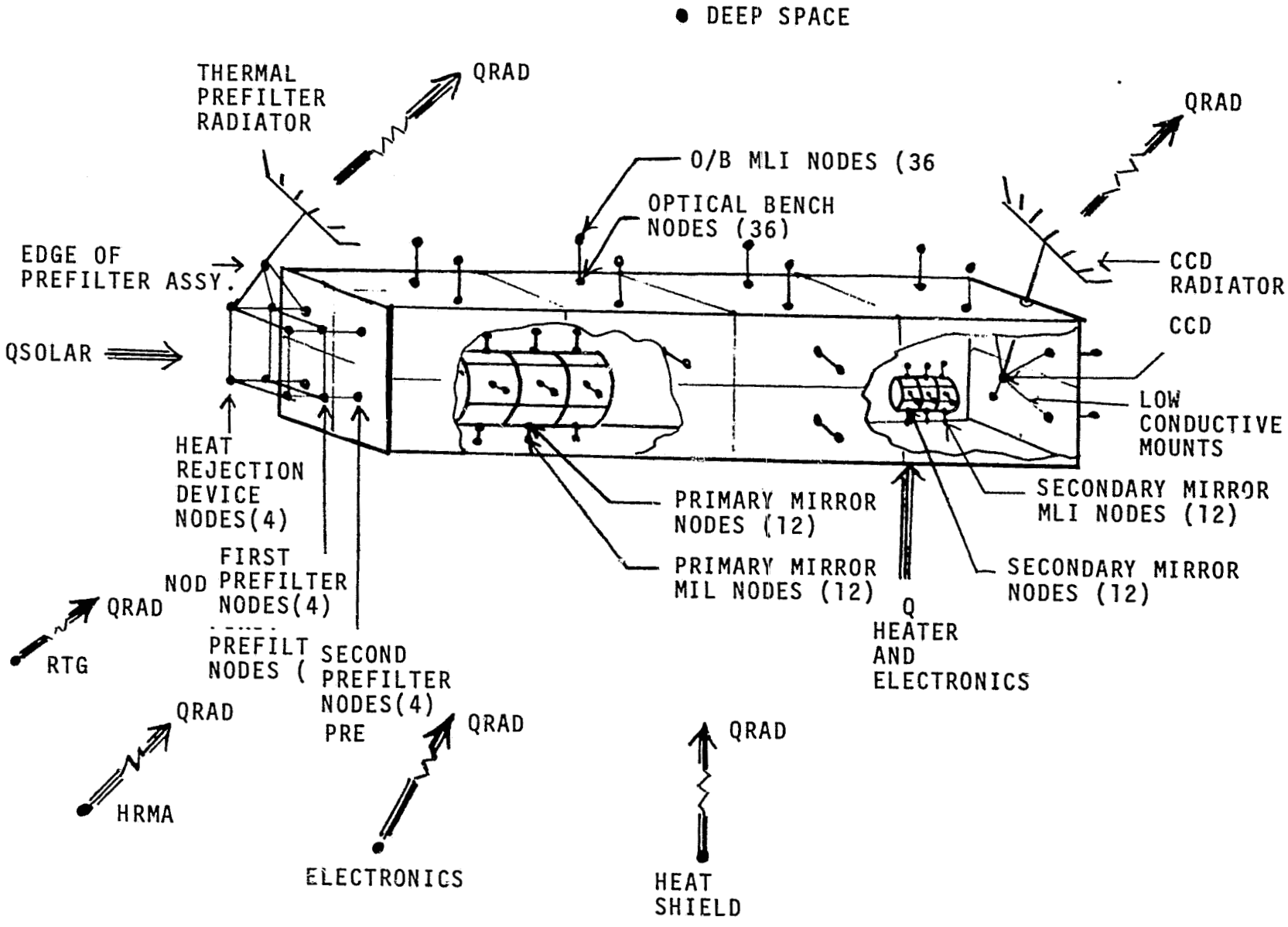

Figure 5-22. Overall System Bench.

TABLE 5-3

Instrument Temperatures and Gradients as a Function of Heater Power

	Temperatures in °C			
	Q = 2.34 Watts	4.68 Watts	11.69 Watts	23.38 Watts
Bench Avg. Temp.	70.6	78.9	100.6	130.0
Bench Side-Side Gradient	0.086	0.079	0.071	0.069
Bench End-End Gradient	9.09	4.67	5.98	22.65
Primary Mirror Avg. Temp.	78.3	85.0	102.8	128.3
Primary Mirror Side-to-Side Gradient	0.020	0.015	0.008	0.035
Primary Mirror End-to-End Gradient	0.511	0.505	0.490	0.461
Secondary Mirror Avg. Temp.	58.3	68.3	96.1	134.4
Secondary Mirror Side-to-Side Gradient	0.013	0.015	0.015	0.018
Secondary Mirror End-to-End Gradient	0.025	0.028	0.036	0 .047
CCD Temperature	-89.0	-80.0	-54.8	-15.0

of thermal soaks, the choices for the mirror and bench materials were limited to materials with similar coefficients of thermal expansion (CTE). A summary of errors from five sources is given in Table 5-4. The sources are:

1. A temperature difference between two sides of each of the mirror sets. Each mirror set deforms from a straight to a curved cylinder.
2. A gradient between the two ends of the primary mirror set.
3. An end to end gradient in the magnifying mirror set.
4. A change in the temperature throughout the entire telescope. This error results from the mirror growing radially at a rate different from its mounts. The analysis assumed that the mirror bulkhead is rigid.
5. A difference in temperatures between the primary and magnifying sets.

As can be seen from the results in Table 5-4 the distortions due to the thermal soak dominate the effects on the resolution. Since it is much easier to minimize thermal gradients in the system than it is to minimize bulk temperature, it is desirable to mechanically isolate the mirrors from the bench by means of radial flexures which would allow differential radial growth between the optical bench and mirrors without imparting excessive loads on the mirrors and thus distorting them. This is a relatively straightforward and well tested solution and should not impose any major problems.

The data from these analyses are used in the determination of acceptable thermal limits, i.e., for a beryllium mirror, a side-to-side temperature gradient most strongly affects the resolution. To keep this source from influencing the resolution of the total instrument, this gradient must be kept below 0.01°C.

Provided adequately sized radiators are available (1 ft^2) the CCDs can be maintained at a temperature of order -90°C which our experience shows is adequate.

TABLE 5-4

Thermal Effects on System Resolution

	*Resolution in Arc-Seconds
Side-to-Side Gradient - Primary Mirror	.673
End-to-End Gradient - Primary Mirror	.122
End-to-End Gradient - Secondary Mirror	.001
Thermal Soaks	33.063
Mirror-to-Mirror Difference	.396
Total (Square root of the sum of squares)	33.072 Arc-Seconds
SRSS Total excluding Thermal Soak	.790 Arc-Seconds

* Described as RMS blur circle diameter.

The operating temperature of the instrument package that results from this design is quite high. The actual temperature distribution depends upon the temperature of the rear of the secondary heat shields. The preliminary JPL thermal model had established the limits on this temperature to be 50 - 100°C. To be conservative we have used the upper end of this range. Any reduction in its value would produce a corresponding reduction in the temperature of the X-ray instrument. In the worst case, where the upper limit is the actual temperature of the shields, we believe it would be possible to lower the temperature of the instrument by conductively coupling the front of the bench to a deep space radiator. However until the thermal environment at the rear of the secondary shields is better known additional work in this area is not warranted.

5.6 Conclusions and Recommendations

The conclusions and recommendations of the structural and thermal analysis are summarized below.

1. The thermal prefilters should be made of beryllium with either copper or silver mesh wire support. The mesh size should be between .025" and .05" with a mesh wire diameter of 7.5% of the mesh spacing.

2. The heat rejection mirror should be 3" in diameter to allow a viewing annulus compatible with the X-ray mirror.

3. The primary heat shield aperture should be as small as possible compatible with the viewing annulus.

4. The optical bench and mirrors should be made of beryllium.

5. A heat rejection device should be employed in front of the prefilters to minimize heat loadings.

6. The mirrors should be mechanically decoupled from the optical bench by means of flexures to minimize distortions in the mirrors during a thermal soak.

7. A minimum of 6.00 watts (3.5 for electronics + 2.5 for heaters) should be provided.

8. The prefilters and CCD's should be cooled by means of 1 ft^2 aluminum radiators with clear views to deep space.

6.0 GENERAL CONCLUSIONS

The purpose of the study was to determine whether an X-ray imaging instrument could be designed to survive the STARPROBE environment. Our analyses indicate that we can answer this question in the affirmative. The baseline design does depend on the development of new technology but where new technology is proposed it is to enhance the scientific objectives not to ensure survivability.

The telescope consists of two grazing incidence mirrors. The second, diverging mirror is located in front of the primary focal plane and magnifies the primary image by extending the effective focal length of the system. CCD cameras are provided at both the primary and secondary foci and both are used to achieve the scientific objectives. This combination will provide a spatial resolution (two pixels) of 20 km at perihelion which is approximately 40 times better than the best resolution achieved to date from earth orbit.

Exposure times would be less than one second.

The major question at the start of the program was the design of the prefilters and whether they could be made to survive the thermal loading. By going to a beryllium prefilter mounted on a silver mesh, a technology which is available, the prefilters have a comfortable safety margin and the design of the rest of the instrument can proceed in a normal fashion

The proposed soft X-ray telescope could be contained within a volume of dimensions 1.80 m x 0.3 m x 0.3 m. The mass of the instrument including a 23% overall contingency is estimated to be 21 kg. The power required, including heaters, is estimated at 6 W although a safer number for planning purposes would be 10 W.

If future studies are commissioned several general topics should be considered before detailed instrument designs are prepared. The most

important of these is a study of the time varying thermal problem covering the range of ± 10 hours about perihelion. This study should include a more thorough evaluation of the environment behind the heat-shields. The model should include feedback from the preliminary designs for the X-ray and Visible/UV telescopes. A knowledge of this environment is crucial to determining the final temperatures of the imaging instruments.

Little consideration was given to the observation sequences that would be required to satisfy the scientific objectives. Since these affect the telemetry and pointing requirements they must be established to determine if they have a major impact on the spacecraft.

The thermal models used in the study relied upon several radiating surfaces with a clear view of deep space. Although the area of these surfaces was not large, they would almost certainly be competing for the available solid angle with radiators from other instruments. To determine if the X-ray instruments requirements can be met a detailed design of the whole spacecraft must be made.

In summary we have uncovered no reason why an X-ray imaging instrument cannot be designed to survive the STARPROBE environment. The spatial resolution of the information recorded by the baseline design would be at least a factor of 10 better than can reasonably be expected from earth orbit. This information, together with the companion data provided by the accompanying instruments, would lead to a more profound understanding of the structure and dynamics of the solar atmosphere.

REFERENCES

1. Design Study of Imaging Techniques for the STARPROBE Mission, Ball Aerospace Systems Division, Boulder, CO, Final Report F81-08, 1981.

2. Report of the STARPROBE Ad Hoc Committee on Imaging, A.B.C. Walker, ed., 1981.

3. Chase, R.C., Davis, J.M., Krieger, A.S., and Underwood, J.H.: "Grazing Incidence Relay Optics," SPIE 316, 1981.

4. Davis, J.M., Krieger, A.S., Silk, J.K., and Chase, R.C.: "Quest for Ultrahigh Resolution in X-Ray Optics," SPIE 184, 96, 1979.

5. VanSpeybroeck, L.P. and Chase, R.C.: "Design Parameters of Paraboloid-Hyperboloid Telescopes for X-Ray Astronomy," Applied Opt. 11, 440, 1972.

6. Vaiana, G.S., VanSpeybroeck, L., Zombeck, M.V., Krieger, A.S., Silk, J.K., and Timothy, A.: "The S-054 X-Ray Telescope Experiment on Skylab," Space Sci. Instru. 3, 19, 1977.

7. Burstein, P., Krieger, A.S., Vanderhill, M.J., and Wattson, R.B.: "Soft X-Ray Imaging Experiments with Charged Coupled Devices (CCDs) and some Astronomical Applications," SPIE 143, 114, 1978.

MATERIAL PROPERTIES APPENDIX 1

Material	Young's Modulus in PSI	Yield Stress in PSI	Ultimate Stress in PSI	P.E.L. in PSI	Density in lb/in^3	Coefficient of Thermal Expansion in 10^{-6} in/in°F	Thermal Conductivity in BTU/ft/°F	Melt Temperature in °F	Endurance - Limit in PSI
Beryllium @ 70°F	44×10^6	-	65,000	8,000	.065	6.2	116.	2330	35,000
Beryllium @ 1000°F	44×10^6	-	-	-	.065	11.6	51.	2330	-
Aluminum @ 70°F	10×10^6	-	9,500	10,000	.100	12.8	137.	1220	4,000
Aluminum @ 1340°F	10×10^6	-	-	-	.100	18.9	127.	1220	-
Quartz	10×10^6	-	-	3,000	.070	.5	.8	-	-
Graphite/Epoxy	14.7×10^6	-	-	20,000	.065	$\pm$.05	22.	-	-
Nickel	28×10^6	-	-	-	.322	7.5	-	-	-
Gold	12×10^6	-	19,000	-	-	7.9	172.	1945	-
Silver	11×10^6	8,000	22,000	-	-	10.9	242.	1761	-
Copper	17×10^6	10,000	32,000	-	-	9.8	226.	1981	-